Evidence of Quaternary transtensional tectonics in the Nekor basin (NE Morocco)

Journal:	*Basin Research*
Manuscript ID	BRE-055-2015.R2
Manuscript Type:	Original Article
Date Submitted by the Author:	n/a
Complete List of Authors:	Lafosse, Manfred; Sorbonne Universités, UPMC Univ Paris 06, CNRS, Institut des Sciences de la Terre de Paris (iSTeP) d'Acremont, Elia; Sorbonne Universités, UPMC Univ Paris 06, CNRS, Institut des Sciences de la Terre de Paris (iSTeP) Rabaute, Alain; Sorbonne Universités, UPMC Univ Paris 06, CNRS, Institut des Sciences de la Terre de Paris (iSTeP) Mercier de Lépinay, Bernard; Géoazur, CNRS-Université de Nice-Sophia Antipolis, Ammar, Abdellah; Faculté des Sciences, Université Mohammed V, Rabat, Morocco tahayt, abdelilah; Scientific Institute, Mohammed V-Agdal University, Gorini, Christian; Sorbonne Universités, UPMC Univ Paris 06, CNRS, Institut des Sciences de la Terre de Paris (iSTeP)
Keywords:	strike-slip basins, Quaternary tectonics, Back-arc basins, Active tectonics, High resolution seismic reflection profiles, swath-bathymetry, Al-Hoceima

Evidence of Quaternary transtensional tectonics in the Nekor basin (NE Morocco)

Manfred Lafosse[1], Elia d'Acremont[1], Alain Rabaute[1], Bernard Mercier de Lépinay[2], Abdelilah Tahayt[3], Abdellah Ammar[4], Christian Gorini[1]

[1] Sorbonne Universités, UPMC Univ Paris 06, CNRS, Institut des Sciences de la Terre de Paris (iSTeP), 4 place Jussieu 75005 Paris, France

[2]Geoazur, CNRS-Université de Nice-Sophia Antipolis, France

[3]Institut Scientifique, Université Mohammed V, Rabat, Morocco

[4]Faculté des Sciences, Université Mohammed V, Rabat, Morocco

***Corresponding author:** Manfred Lafosse

Address: Institut des Sciences de la Terre – Université Pierre et Marie Curie

Address: 4 place Jussieu, 75005, Paris, France

Tel: +33(0) 1 44 27 59 43

Email:manfred.lafosse@upmc.fr

Abstract

The geodynamic processes in the western Mediterranean are driven by both deep (mantle) processes such as slab-rollback or delamination, oblique plate convergence and inherited structures.

The present-day deformation of the Alboran Sea and in particular the Nekor basin area is linked to these coeval effects. The seismically active Nekor basin is an extensional basin formed in a convergent setting at the eastern part of the Rif Chain whose boundaries extend both onshore and offshore Morocco. We propose a new structural model of the Nekor basin based on high-resolution offshore data compiled from recent seismic reflection profiles, swath bathymetry acquisitions, and industrial seismic reflection profiles. The new dataset shows that the northern limit of the basin is oriented N49° with right-stepping faults from the Bousekkour-Aghbal fault to the sinistral Bokkoya fault zone. This pattern indicates the presence of an inherited left-lateral basement fault parallel to the major inherited Nekor fault. This fault has been interpreted as a Quaternary active left-lateral transfer fault localized on weak structural discontinuities inherited from the orogenic period.

Onshore and offshore active faults enclose a rhombohedral tectonic Nekor Basin. Normal faults oriented N155° offset the most recent Quaternary deposits in the Nekor basin, and indicate the transtensional behaviour of this basin. The geometry of these faults suggests a likely rollover structure and the presence at depth of a crustal detachment. Inactive Plio-Quaternary normal faults to the east of the Ras Tarf promontory and geometries of depocentres seem to indicate the migration of deformation from east to west. The local orientations of horizontal stress directions deduced from normal-fault orientations are compatible with the extrusion of the Rifian units and coherent with the westward rollback of the Tethyan slab and the localization of the present-day slab detachment or delamination.

Key words: Quaternary tectonics; Active tectonics; Al Hoceima; high-resolution seismic reflection profiles; swath-bathymetry; strike-slip basins, back-arc basin.

Introduction

Oblique convergence introduces poorly understood complexity to the structural evolution of back-arc basins.. There can often be described an interplay of strike-slip partitioning and extensional faulting, along with compressional tectonics (e.g. Taymaz, e.g. 1991; Allmendinger et al. 1997). In this interesting context where major transfer fault zones develop, the driving dynamics controlling the style and accommodation of the deformation of the continental crust may not only be the large-scale plate kinematics, but can also include the effects of crustal heterogeneities as well as deep processes in the upper mantle (Teyssier, et al. 1995; Dewey 2002; Jolivet, et al. 2009; Curren & Bird 2014; Faccenna et al. 2014). In this paper, we address two critical questions: If these processes are concomitant, how do they affect the localization and the style of the regional deformation, and can we unravel their specific roles in the surface deformation.

One best studied analogue in the Tethyan domain is the Vienna Basin at the Eastern Alpine-Carpathian junction, where the Eurasia/Apulia convergence resulted in the tectonic escape of the North Pannonian Unit. Slab roll-back led to the formation of transfer faults crossing older thrusts of the Carpathian orogen (Ratschbacher et al. 1991; Wortel 2000; Hölzel et al. 2010). Local extension and regional stress field rotation produced the transtensional Vienna basin by reactivation of the inherited thrusts of the Carpathian orogenic arc (Fodor 1995; Decker, et al. 2005).

In the western Mediterranean, and particularly in the Alboran Domain, evidences for the importance of structural inheritance and mantle processes, such as slab-rollback or delamination, in large-scale geodynamics are accumulating (e.g. Jolivet et al. 2009; Perouse et al., 2012). Squeezed between the Eurasia and the Africa plates, the Alboran Domain includes both the internal part of the Betic-Rif arcuate orogenic belt and the Alboran Basin thinned by back-arc extension (Fig. 1A). In this Domain, the relative amount of back-arc extension and oblique convergence together with upper mantle and crustal heterogeneities control the deformation. Indeed, vertical movement associated to crustal thinning and continental lithosphere removal could be explained by mantle delamination under the Alboran Domain (Seber et al. 1996; Platt et al. 1998; Calvert et al. 2000; Thurner et al. 2014; Levander et al. 2014). Moreover, roll-back of a small portion of a Tethyan slab could be coupled at its top to the southern margin of Alboran Domain and dragged the Betico-Rifian block toward the SW (Fig 1B) (Perouse et al. 2010). In this complex setting where deep processes are known, the Trans-Alboran Shear Zone (TASZ, de Larouzière et al, 1988) is a set of *en echelon* wrench faults running from Iberia to Morocco that accommodate the continuous oblique convergence between Africa and Eurasia (Fig.1A-B).

Along the TASZ, changes in plate kinematics coupled with block rotation along strike-slip faults (De Larouzière et al. 1988; Campillo, et al. 1992; Morel & Meghraoui 1996; Herraiz et al. 2000; Calais, et al. 2003; Martínez-García et al. 2013) have led to the formation of a present-day intra-plate NNE-SSW segmented left lateral shear zone crossing the Miocene structure of the Alboran Domain, materialized by the Adra and Al-Idrissi faults, and propagating southward and northward since the Pliocene (Martínez-García et al. 2013)(Gràcia et al. 2006; Ballesteros, et al. 2008; Martínez-García, et al. 2011; Martínez-García et al. 2013; Estrada et al. 2014; Vázquez et al. 2014) (Fig. 1A).

The area studied in this contribution is the transtensional Nekor Basin located near the city of Al-Hoceima (Morocco), south of the Al-Idrissi fault zone and at the transition of crustal thickening recorded between the Betico-Rifian Block and the Eastern part of the Alboran Domain (Fig. 1B-C) (e.g. Mancilla & Diaz 2015; Petit et al. 2015). The Nekor basin is at the junction between the TASZ and the N050° Nekor fault (Aït Brahim and Chotin 1990; Asebriy et al. 1993), which plays as a lateral ramp (Tahayt et al. 2008 and Koulali et al. 2011). The studied area is known for its important seismicity (Fig. 1B) with periodically large magnitude earthquakes (Mw=6.0 and Mw=6.4 in 1994 and 2004, respectively) (El Alami et al. 1998; Bezzeghoud & Buforn 1999; Jabour et al. 2004; Stich et al. 2005; Medina & El Alami 2006; Cakir et al. 2006; van der Woerd et al. 2014).

The Marlboro-2 and SARAS surveys in 2012 (d’Acremont et al. 2014; d'Acremont et al. 2013) provided a new set of high resolution multibeam bathymetry and two-dimensional seismic reflection profiles between the Ras Tarf volcanic province and the Alboran internal units (Figs 1C). Active faults on the shelf are mapped thanks to the tight coverage of the seismic and bathymetry survey. Previously published industrial data (e.g. Calvert et al. 1997) are reinterpreted using these new data. Our methodology allows us to map the present-day deformation and its distribution through time (Fig. 2). It revealed the offshore tectonic boundaries of the basin. Horizontal stress orientations deduced from recent conjugate normal faulting are compared to the results obtained from the inversion of moment tensors. Our results have implications for the understanding of the evolution of a transtensional basin in a convergent setting where upper mantle processes occur. We discuss the role of plate kinematics, mantle dynamics, and inheritance on the development of large strike-slip faults and propose that lateral slab migration could be the main controlling factor for surface deformation.

Geological setting

The Rif Orogenic belt consists of stacked south verging nappes: the internal Rif units, the Flysch units, and the external Rif units, the latter composed of the Intra-Rif, Mesorif and pre-Rif (Fig. 1C). The internal units were emplaced during the Eocene-Oligocene Alpine-style tectonic phase (Chalouan et al., 2008). The Flysch unit, locally known as the Tisirene nappe, consists of Jurassic to Oligocene oceanic sediments overlain by turbiditic clastic deposits of Chattian-Aquitanian age. The external Rif units consist of stacked low-grade to non-metamorphosed sedimentary cover. Early Cretaceous detrital sediments, and Albian-Aptian turbiditic formation compose the Intra-Rif locally called Ketama Unit (Fig. 1C; Asebriy et al., 1987). This unit overlies the serpentinized lherzolites and green schist metabasites of the Beni-Malek massif (Fig. 1A; Michard et al., 1992). Toward the south, the structural units known as the Mesorif (locally called, the Temsamane Unit) and the Prerif Units complete the external Rif (Fig. 1A-C).

Slab retreat triggered the E-W back-arc extension of the Alboran domain until Early Tortonian, followed by the tectonic inversion of the Alboran Basin around 8Ma under the effect of the Africa/Eurasia convergence (Jolivet et al. 2008). The compression of the continental crust was partially accommodated along the Xauen and Tofino banks and the Alboran Ridge, a present-day submarine high crossing the Alboran sea with a NE-SW direction (Fig. 1A; Campillo, et al. 1992; Bourgois, et al. 1992; Mauffret, et al. 1992; Woodside & Maldonado 1992; Comas et al. 1999). Plio-Quaternary regional oblique convergence triggered anti-clockwise rotations of the stress-field directions relative to the Late Miocene transpressive structures (De Vicente et al. 1996; Lonergan et al. 1997; Galindo-Zaldívar, et al. 1993; Aït Brahim & Chotin 1990). On the Alboran Ridge, the folding of the Messinian Unconformity, and the deformation of younger stratigraphic surfaces, coincident to higher sediment depositional rates in the South Alboran Basin, show tectonic pulses due to regional shortening at 5.33-4.33Ma, 3.28-2.45Ma and 1.81-1.19Ma (Martínez-García et al. 2013). The Al-Idrissi fault accommodated significant although not quantified left-lateral displacement during the last tectonic pulse at 1.81-1.19Ma (Martínez-García et al. 2013), and offsets the seafloor (Munoz et al. 2008; Martínez-García et al. 2011).

The Nekor sedimentary basin is located at the southern tip of the TASZ, south of the Al-Idrissi fault (Fig. 1C). Its northern boundary, the Bokkoya fault, has been hypothesized either as a normal left-lateral strike–slip fault (Calvert et al., 1997; El Alami et al., 1998, van der Woerd et al., 2014), or as a normal fault (Mauffret et al., 2007). To the west, the left lateral Bousekkour-Aghbal fault crosses the shoreline with a N020° direction and offsets the seafloor (d'Acremont et al. 2014). The uplift of the Quaternary abandoned alluvial terraces indicates a vertical motion along the Ajdir fault, and the northern segment of the NW-SE Imzouren fault (Fig. 1C), together with the activity of the N-S Rouadi fault and the El-Hammam fault to the West (van der Woerd et al. 2014). The N005°

W70° S60° normal Trougout fault partly accommodates the local extension since Plio-Quaternary times (Aït Brahim and Chotin 1990). Recent results in tomography and field studies show that the - Trougout and the Bou-Haddad faults are continuous and connect with the Nekor fault to the south (Fig. 1C; Poujol et al., 2014, van der Woerd et al. 2014). Between the Ketama and the Temsamane Unit, the Nekor fault is early Tortonian to Messinian in age, with a N050° trend (Leblanc & Olivier 1984; Asebriy et al. 1993; Negro et al. 2007). This major left-lateral strike-slip fault is considered as the southern boundary of the Nekor basin, and has accommodated 50km of lateral displacement during the E-W Miocene extension (Leblanc & Olivier, 1984). Plio-Quaternary deformation recorded in sediments onshore in the Boudinar and in the Nekor basins indicates a Plio-Quaternary E-W to ENE-WSW extension (Aït Brahim and Chotin 1990; Asebriy et al. 1993; Galindo-Zaldívar et al. 2015). Several field studies have proposed that only the segment of the Nekor fault located west of the Bou-Haddad fault is still active today (Hatzfeld et al., 1993; Poujol et al., 2014; van der Woerd et al., 2014).

An interpretation of a gravity profile indicates that the basement in the Nekor basin is tilted eastward towards the Trougout fault (Galindo-Zaldívar et al. 2009), and is filled with a 400 m thick Plio-Quaternary sequence overlying undated marls (Aït Brahim 1985). These deposits unconformably overlie the Ketama units. The Ras Tarf high, a -15 to -9Ma aged andesitic-basaltic province, is the eastern boundary of the Nekor basin (Fig. 1C) (Duggen et al. 2004; El Azzouzi et al. 2014). Relics of a Messinian reef, now located at 588m above the sea level, show the uplift of this volcanic province (Ammar et al. 2007). Ammar et al. (2007) estimated an average regional uplift rate of 0.2 mm/yr since the Messinian. Poujol et al. (2014) proposed a regularly decreasing uplift rate for the Ras Tarf province, from about 0.45 mm/yr 500 ky ago, to 0.2 mm/yr between 200ky and 120ky ago, and to 0.13 mm/yr since 120ky. Most recent field studies found NWW-SSE extensional structures affecting the Messinian and Pliocene sediments (Galindo-Zaldivar et al. 2015). The beginning of subsidence inside the Nekor basin has not been accurately dated. Morel (1988) and Poujol et al. (2014) assumed that the subsidence began during the Quaternary.

Recent works of van der Woerd et al. (2014), d'Acremont et al. (2014) and Galindo-Zaldívar et al. (2015) hypothesize that local normal faults branch on a common crustal detachment level at the base of the Nekor basin. Onshore, the Nekor basin southern boundary follows the Nekor fault, which suggests that crustal anisotropies control the geometry of the basin and constrain the present-day seismicity (Poujol, et al. 2014; van der Woerd et al. 2014; Galindo-Zaldívar et al. 2015).

Recent deformation

At present-day, kinematic data show a lateral escape of the Betico-Rifian block toward the SE with respect to the Africa plate (Vernant et al. 2010; Koulali et al. 2011; Palano et al. 2013). From GPS data, the Betico-Rifian block motion toward the south-west is 1mm/y greater than the ~4 mm/year Africa/Eurasia convergence (Nocquet 2012; Palano, et al. 2013). Studies of the regional seismicity have mostly located hypocentres within the first15 km of the crust, and between the Bousekkour-Aghdal and the Trougout faults (e.g. Calvert et al. 1997; Tahayt et al. 2008). Calvert et al. (1997) studied the local seismicity and 2D seismic profiles in the offshore part of the Nekor basin. They described an onshore-offshore N-S basin which transfer the deformation from the Alboran Ridge to the North to the Rifian units and the Nekor Fault to the south (Fig. 1A).

Inversion of the moment tensors of the main shocks of the 1994 and 2004 events indicates a strike-slip motion (Fig. 1C). Part of the seismicity related to these events is located offshore (Medina 1995; Bezzeghoud & Buforn 1999; Stich 2003; Stich et al. 2006; Jabour 2004; van der Woerd et al. 2014; Calvert et al. 1997). D'Acremont et al. (2014) found that the Bousekkour-Aghbal N020° fault trace on the seafloor matches with the location of one of the hypothesized epicentres of the 1994 earthquake (Fig. 1C). Onshore field studies following the 2004 earthquake showed cracks through the Tisirene Flyschs and the Ketama units, with a general orientation of σ3 around N40° (Aït

Brahim et al. 2004; Tahayt et al. 2009; Galindo-Zaldívar et al. 2009). However, no clear primary surface rupture can be observed (Akoglu et al. 2006; Biggs et al. 2006). Galindo-Zaldívar et al. (2009) proposed that this could be the results of overlying detachments blinding the fault. From the inversion of moment tensor, most of the authors agree on a local strike-slip stress field near Al-Hoceima with a Sh_{max} roughly oriented N150°±20° (Medina 1995; Calvert et al. 1997; El Alami et al. 1998; Bezzeghoud & Buforn 1999; Stich et al. 2005; Stich et al. 2006; Stich, et al. 2010; Palano, et al. 2013; Ousadou et al. 2014; Van der Woerd et al. 2014) and a NE-SW direction of extension, in accordance with N145° open joints found in Quaternary breccia near the northern tip of the Imzouren fault (Galindo-Zaldívar et al. 2015). The seismicity and the modelling of the local stress field show that the latter is rotated around Al-Hoceima with respect to the far field stress direction given by direction of Eurasia/Africa convergence (Fadil et al. 2006; Fernández-Ibáñez et al. 2007; Perouse et al. 2010; Pedrera et al. 2011; Cunha et al. 2012; Palano, et al. 2013; Ousadou et al. 2014). This rotation implies a local effect of crustal structures on the stress field.

Data and methodology

In the present study, three academic surveys (Marlboro-1, Marlboro-2, SARAS) explore the continental shelf in the vicinity of Al-Hoceima (d'Acremont, et al., 2013; d'Acremont et al., 2014), with a combination of two-dimensional seismic reflection profiles, a topographic parametric sonar (TOPAS) sub-bottom profiler and multibeam bathymetry (Fig. 2).

During the Marlboro-1 cruise on board the *R/V Côtes de la Manche*, high-resolution seismic reflection data were recorded using a mini-GI air gun and a 12-channel streamer. During the Marlboro-2 cruise on board the *R/V Téthys II*, shallow-water swath bathymetry (Reson 8101 system) and very high-resolution seismic reflection profiles (sparker source, six-channel streamer) were acquired (d'Acremont et al., 2014). During the SARAS cruise on board the *R/V Ramon*

Margalef, swath-bathymetry (EM710 system) and high and very high resolution seismic reflections (sparker source, six-channel streamer, TOPAS full ocean depth hull-mounted system, respectively) were acquired. This comprehensive acoustic dataset was combined with the available industrial data, which allowed the imaging of the deep to shallow sedimentary filling of the basin with a good compromise between penetration (P) and resolution (R): TOPAS, R = 10 cm, P = 200 m; sparker, R = 1 m, P = 30 m; academic 12-channel streamer, R = 5 m, P = 100 m; and industrial multi-channel streamer, R = 15 m, P = 500 m. The swath bathymetry (Fig.1C) had a definition of 25 m^2 per pixel, while its vertical resolution was around 0.5 m for water depths below 100 m.

The morpho-bathymetry analysis identified tectonic-related scarps on the seafloor (Fig. 1). Following Nash (2013), linear topographic features at the seafloor are interpreted as fault scarp. Boundary faults of the Nekor basin are visible at the seafloor (d'Acremont et al. 2014), although faults with vertical displacement rates inferior to the sedimentation rate might not be visible (e.g. Barnes & Pondard, 2010). Independently, we plotted the fault traces along the seismic profiles. As the number of faults per profile is high (a total of 4,309 faults were plotted along all seismic profiles), and the distance between the lines is small (varying from 250m to 500m), it is possible to follow the faults across adjacent profiles. For that purpose, we separately plotted the faults dipping west and the faults dipping east (Fig. 2, and following seismic profiles). The apparent fault dip was computed assuming a simple P-wave velocity model of 1,550 m/s for the sedimentary cover. As the depth of acquisition remained shallow (two-way travel time[twtt] $\leqslant$ 250 ms), we considered the compaction to be negligible and the P-wave velocity of the shallow sediments to be close to that of water (water column measurements performed during the Marlboro-2 and SARAS cruises give a water velocity of around 1,510 m/s). We tentatively fixed the apparent fault dips by considering the angle between the azimuth of the fault trace on the seafloor (or the interpreted continuous fault segment on successive seismic profiles) and the direction of the seismic profiles.

Despite the tight seismic coverage, there are some methodological and interpretative biases to highlight: to the West of the Nekor basin, the structural map is difficult to complete on the inner shelf due to the poor penetration of P-waves in the sub-outcropping basement under the thin sedimentary cover. Moreover some faults may be parallel to the ship track and may not cross seismic profiles, or cross with low angles (<20°). However the main active normal faults accumulate the most vertical offset observed on the seismic profiles and match with the fault track deduce from the bathymetry. As we cannot observe measurable lateral displacement on the sampled faults, we cannot evidence oblique slip. Consequently, faults described hereafter are described has apparent normal faults. The interpolation of morpho-bathymetric features and seismic reflection data analyses led to a new structural map of the studied area (Fig. 3).

<u>Seismic facies and morphology of the shelf</u>

To the north of the studied area, we observe three seismic units on the MAB258 profile (Fig. 4). Unit 1 (U1), the basal strata, is characterized by transparent seismic facies with low-amplitude reflections of undetermined thickness. Unit 2 (U2) is a succession of high-amplitude and low-amplitude continuous reflectors and with its top marked by an unconformity surface (x-distance: 12.8km-16km; Fig. 4). Unit 3 (U3) is characterized by medium-amplitude high-frequency continuous reflectors, from the shelf to the basin. On the shelf, the base of Unit 3 is defined by aggrading-prograding sigmoid clinoforms, evolving upwards to prograding oblique-tangential clinoforms at the top of the unit. The respective thicknesses of U2 and U3 increase gently towards the east. U2 is pervasively cut by normal faults with tens of meters in spacing. Some of these faults offset the unconformity surface, but do not reach the seafloor.

From the correlation between seismic reflectors in the south Alboran basin and the ODP drill Site 979, Martínez-García et al. (2013) described the succession of three Quaternary seismic facies: (1)

Q3 is semi-transparent with amplitudes increasing toward the top and represents the base of the Quaternary (between 1.81-1.19Ma), (2) Q2 is a set of continuous parallel high-amplitude reflectors which represents the 1.19-0.79Ma period and (3) Q1 is a set of moderate to high amplitude reflectors which represents the 0.79Ma-Present time period. We propose from seismic facies correlation that U1, U2, and U3 facies correspond to the local representation of Q1, Q2 and Q3 respectively. Therefore, we date the transition between U2 and U3 around 0.79Ma (orange surface on seismic profile figure 4).

On the western part of the Nekor basin, the top of the acoustic basement is characterized on the seismic reflection lines by three high-amplitude low-frequency continuous horizons that correspond to a strong impedance contrast between the acoustic basement and the Plio-Quaternary shelf (Fig. 5, 6, 7, 8). On the eastern part of the basin, the acoustic basement visible on the MAB281 correspond to the sharp transition between a transparent facies associated to volcano-clastic deposit from the Ras Tarf volcanic massif, and a parallel reflector from the Plio-Quaternary shelf (x-distance; 21.5km; fig. 9)(d'Acremont et al. 2014).

Oscillation of the eustatic sea-level may influence the recognition of the fault trace on the shelf. As in many areas over the Mediterranean (e.g. Lobo and Ridente 2014), the shallow Quaternary shelf in the Al-Hoceima region shows a succession of prograding and aggrading seismic units (e.g. Fig. 6). A tectonic influence is visible in the sedimentary record. On the western part of the seismic line (Fig. 7), from either part of a recent N163° W70° fault called A, variations of seismic reflector packages thickness (considering that the sediments flux is stable during this time interval) show the contrasts of subsidence rates in the Nekor basin: variations of thickness indicate that accommodation space is more important in the western part of the bay, where the subsidence is faster than in the eastern part.

At the seafloor, the shelf break is around 125 metres below sea level (mbsl) in front of the Ras El Abid, the Ras Tarf and in the Nekor bay, and marks the transition between the slope toward the deep basin and the continental shelf (Figs 10, 11 and 12). Above the shelf break, we observe a succession of scarps parallel to the shelf break limiting flat surfaces (Figs 4 and 9AB). The 125m isobath is the maximum value of sea level fall after Rabineau et al. (2005). Above 125mbsl, the shelf was exposed to aerial and sub-aerial erosion during the last lowstand period at the Last Glacial Maximum (LGM times). The marine terraces observed at the vicinity of Al-Hoceima likely mark several standstills during the rise of the last transgression (e.g. Rabineau et al. 2005; Zecchin et al. 2015). The presence of those marine terraces (noted as *t* on Figure 11) implies that the tectonic features at the seafloor located above 125mbsl were subject to wave ravinement and sub-aerial or aerial erosion since the last lowstand (Zecchin et al. 2015). As a consequence, tectonic features under the 125mbsl are likely to be less affected by erosion, but may be masked by more important sediment accumulations at the last lowstand period.

Morphotectonic features

The Bousekkour-Aghbal fault zone

The fault trace of the Bousekkour-Aghbal fault at the seafloor is 3.5km long and corresponds to the normal fault F1 (N25°E71° ±14°, Fig. 6 and 11). The footwall of the Bousekkour-Aghbal fault forms a rough patch on the bathymetry and disappears towards the northwest under recent sediments (Fig.11). The maximum offset of the seabed is around 5 m and the apparent offset of the basement at the footwall is 45m (Fig. 4). F1 and F2, together with a buried fault to the west of F1, correspond to right-stepping *en echelon* faults (Fig. 11). Along the fault, the reflector terminations indicate a progressive tilting, and record the continuous deformation of the sedimentary sequence (Fig. 4). The tilt of high-angle prograding reflectors at the top of the sequence (Fig. 6) attests to a recent uplift of the western wall of the F1 fault. To the east, the deformation of the sedimentary cover quickly fades (Fig.11). These faults show the syntectonic sedimentary record of the long-term deformation of the shelf east of Ras El Abid, which was bounded a 2-km-wide en echelon fault zone, with a pronounced normal component.

The Bokkoya fault zone

The figure 12 shows the north-western boundary of the Nekor basin. The F3, F6, F7 faults are *en echelon* and are oriented N032°, N055° and N23° respectively. The most prominent scarp of outcropping basement on the shelf is 2.5 km long and corresponds to F3 (Fig. 7 and 12), which produces a 10m vertical offset of the seafloor and disappears northwards. Further to the northeast, the fault zone corresponds to an elongated NE-SW bulge of the seafloor (Fig. 12) and matches with a 2.5-km-wide flower structure, bounded by the northern prolongation of fault F3 and the southern prolongation of fault F8 (MAB65, Fig. 8). Continuous reflectors of constant thickness overlap the flower structure (MAB65, Fig 8). Offlaps on the draping unit indicate that the uplift rate became progressively greater than the accumulation rate. This complete sedimentary sequence is affected by faulting (Fig. 8), although a sharp seafloor breakup cannot be seen in the bathymetry (Fig.12).

The N029° F8 fault trace (Fig. 12) defines a 4-km-long fault which produces a 44-m vertical offset of the seafloor. F8, F9, F10, F11 are *en echelon* and produces a 1-m vertical offset of the seafloor (Fig. 12).). The western part of profile MAB258 shows the northern prolongation of this NE-SW fault zone (X-distance: 9000-9600m; Fig. 4). The subsidence of the sediments between the walls of the fault zone (F10, F12 Fig. 4) indicates recent extension, while the absence of vertical shift on either side of the fault zone indicates a strike–slip behaviour. The right stepping fault segments F3 to F12 (Fig. 12) form a continuous fault zone which fits with the position of the Bokkoya fault described by Calvert et al. (1997).

Fanning geometries of the seismic reflectors and normal offset of chaotic bodies, interpreted as Mass Transport Deposit (MTD), illustrate the extension in the distal part of the Nekor basin (MAB29, MAB33, Fig. 7 and TOPAS4242, Fig. 10A-B). The fan sequence shows that east-dipping normal faults have affected the entire sedimentary cover (Fig. 7). At the seafloor, the tectonic scarps are however locally attenuated by recent sediment waves (Fig. 7). The NW-SE normal faults distribute the deformation over a 3-km-wide area with a cumulative offset of acoustic basement varying between 114 and 140 ms twtt (Fig. 7; MAB33).

The Trougout fault zone

On the eastern boundary of the sedimentary Nekor basin, a >4m high linear NNW-SSE shift of the seafloor correspond to the N174° W80°±4° normal fault F20 (Figs. 9 and 12). The fault trace progressively disappears toward the north and indicates the tectonic contact between the Ras Tarf volcanic province and the Plio-Quaternary sediments of the basin. F20 fits with the offshore prolongation of the onshore Trougout fault (d'Acremont et al. 2014).

Westwards, secondary scarps striking N126° (F18) and N144° (F19) connect to the Trougout fault (Figs 9 and 12). These normal faults limit a recently subsiding sub-basin (X-distance: 19,900 m to 21,300m; Fig. 9). Several depositional sequences can be followed from the Nekor basin to their terminations against the fault F20 where drag folds at the hanging wall of F20 are compatible with a normal tectonic style (Fig. 9). .The prograding geometry of low amplitude reflectors shows the periodic increase in accommodation space and the oblique filling of the sub-basin limited by F18 and F19 (Fig. 9). Considering constant sedimentary flux, the F18 faults (Fig. 12) appears to have long-term transient activity, which is likely to be related to the activity of the major fault F20.

Weak vertical offset of paleo-channels (X-distance: 16,800 m; Fig. 9) shows either the local strike–slip component of faults that cross the basin, or normal motions along the fault zone that have not cumulated enough vertical offset. This suggests either strike–slip faulting inside the basin or spatio-temporal evolution of the faulting, with more recent normal faults to the west of the MAB281 profile than to the east.

Fault pattern through the offshore-onshore Nekor basin

Through the offshore Nekor basin, F14, F15, F16, and F17 (Figs. 12) are a set of regularly spaced NW-SE west dipping fault traces observed on the seafloor and deviating marine incisions (Fig. 12). The average azimuth of those faults is N151°±6°. These faults produce 1 to 6m vertical offsets with normal component.. The F15 continues southwards as the fault splays through more NS faults and becomes difficult to follow. The F16 fault outcrops as a 4.5-km-long segment. Vertical shifts of the seafloor become harder to observe to the east of F17 where normal faults appear to be capped by a MTD (Fig. 10). At the north-eastern boundary of the Nekor basin, N165° west dipping normal faults form the kilometre-wide northern prolongation of the Trougout fault zone (X-distance: 13,200-15,250 m, burial <10 ms twtt; Fig. 4). Those faults do not shift the seafloor and appear to be buried under 10-20 ms twtt of sediments. At depth, the graben structure within the Nekor basin faults was illustrated previously by Calvert et al. (1997). Shallow normal faults observed on the TOPAS4242 profile could correspond to the normal faults with kilometre in spacing, visible in the deeper penetration IZD29 industrial profile (Fig. 10C).

The new structural map for the offshore Nekor basin is shown in Figure 13. It shows the geometry of the faults across the Nekor basin and along its edges (Fig. 3). Three families of faults can be distinguished (Figs. 3): (1) the Bousekkour-Aghbal fault zone and the Bokkoya fault zone, striking between N25° and N30°;(2) across the basin, the distributed normal faults that strike roughly N160°; and (3) the Trougout N-S fault zone that defines the boundary between the Plio-Quaternary deposits of the basin and the volcanoclastic facies of Ras Tarf (Fig. 3).

In the offshore part of the Nekor basin, NW-SE normal faults affect the seafloor and continue towards the coastline. Those faults are not observed onshore. It could be because (1) the vertical component of the deformation is distributed over a great number of normal faults, lowering the vertical deformation rates of each individual fault; (2) the record of a fault vertical offset has probably been erased by aerial, sub-aerial erosion during lowstands, and soil erosion during the relative sea-level rise (Rabineau et al. 2005; Zecchin et al. 2015); (3) the sedimentary supply onshore is greater that the cumulated vertical deformation on the faults.

Discussion

Inherited fabrics and present-day geometry of the Nekor Basin

To the northwest of the Nekor basin, the Bousekkour-Aghbal and Bokkoya fault zones consists of several right-stepping kilometre-long faults visible at the seafloor (Fig. 13). As we do not observe any major tectonic structure in the northern vicinity of the Bokkoya fault zone, we consider that this fault zone corresponds to the active north-west left-lateral boundary of the Nekor Plio-Quaternary basin. We interpret the 40km long shear as the northern Principal Displacement Zone (PDZ) of the Nekor basin (Fig. 14A) (e.g. McClay and Dooley 1995). The eastern boundary of the Nekor basin is a 45 km-long N-S fault zone running from the Nekor fault to the southern tip of the Al-Idrissi fault and including the Trougout and the Bou Haddad faults (Fig. 14A). Those last two faults are roughly parallel to the El-Hammam fault to the West and together represent the active master faults of the Nekor basin (e.g. Rahe et al. 1998). The geometry of the tectonic Nekor basin is therefore rhombohedral in shape.

Along the northern PDZ, the pattern (e.g. Naylor,et al. 1986) of right-stepping segments over a 20-km-long and 2-2.5 km-wide fault zone, together with a weak vertical offset of the 0.79Ma reflector (Fig. 4) indicate a sinistral kinematic of the shear zone (Fig. 13 and 14). Within the fault zone, the subsidence marks the partitioning of the deformation between the sinistral slip component and the extensional dip–slip vertical component inside the sedimentary cover. The geographic disposition of the NE-SW faults can be interpreted either as *en echelon* R-shear (e.g. Wilcox, et al. 1973), or from recent analogous modelling, as *en echelon* marginal faults in a transtensional pull-apart context (Wu et al., 2009). The compressive flower structure at the southern tip of the Bokkoya fault is related to a restraining step-over between two right-stepping N030° segments, compatible with the sinistral slip of the fault zone (F3 and F8, Fig. 12). Inside the relay, the geometry of the reflector packages is probably due to the combined effects of the distribution of the deformation across the flower structure and the sedimentary supply overcoming periodically the tectonic growth. As shown by analogous modelling (e.g. Naylor, et al. 1986; McClay and Dooley 1995), the un-anastomosed Riedel-shear pattern occurs in the sedimentary cover when the displacement along a basal discontinuity, and the total strain applied on the sand-box model, are small. The similar geometry of the faults observed at the seafloor suggests a recent activation of the Bokkoya fault as a wrench fault. Consequently, we interpret the *en echelon* Bokkoya fault segments as evidence of a inherited crustal-scale fault that strikes N049° (Fig. 14B). As suggested by Calvert et al. (1997), the direction of the Bokkoya fault zone is parallel to the Nekor fault, which therefore corresponds to the southern PDZ (Fig. 14A) (Asebriy et al. 1993). As in many transtensive areas (e.g. Allen et al. 1998 for the Bohai basin; Hölzel et al. 2010 for the Vienna basin, and the review of Mann 2007), it appears that inherited fabrics control the geometry of the Nekor basin. Indeed, the Nekor fault is a major structural limit between the Ketama and Temsamane Units (Fig. 1C) (Chalouan & Michard 2004; Michard et al. 2007; Benzaggagh et al. 2014). Similarly, we propose that the Bokkoya basement fault, which is parallel to the Nekor fault and to the major south-east verging thrust onshore, reuses inherited Alpine thrusts or Tortonian NE-SW wrench faults at depth. The PDZs of the Nekor basin are likely to be localized on weak inherited structural discontinuities.

Structural evolution of the Nekor basin.

The higher subsidence and the intense seismic activity in the western part of the Nekor basin suggest a higher strain in the western area at present-day. East of the Trougout fault, normal faults appear not to offset the seafloor. The depth of the depocentre of the Plio-Quaternary sequence is maximum at the foot of the Trougout fault with a 0.3stwtt vertical offset of the basement (Fig. 10C). The geometry of the basement indicates asymmetric depocentre, in a very similar way to the onshore cross-section that was illustrated by Galindo-Zaldívar et al. (2009).

The extensional deformation of U1 and U2 (Fig. 4) and inactive faults east of the Trougout fault are compatible with the results of onshore field studies showing a Plio-Quaternary E-W extension (e.g. Aït Brahim & Chotin 1990; Galindo-Zaldívar et al. 2015). The extensional deformation of U1 and U2 is distributed over a great number of faults, and is not localized within the present-day limits of the basin (Fig. 4). The age of the units U1 and U2 suggests that the pulse of shortening around 1.81-1.19Ma on the Alboran Ridge and in the South Alboran Basin is concomitant with the observed extension in the Nekor basin (Martínez-García et al. 2013). This tectonic episode seems to be over around 0.79Ma (orange surface Fig. 4), when the deformation of U3 is localized on the Trougout fault zone at the north of the Nekor basin and on the Bokkoya fault zone (Fig. 4). The thickness variation of reflector packages indicates that the subsidence becomes then more important in the western part of the Nekor Bay than in the eastern part (Fig. 5).

The families of NW-SE and R-Shear produce the most important vertical offsets of the seabed and of the basement in the vicinity of Bokkoya fault zones where the most important amount of the seismicity is recorded (Figs. 1B). Eastward, the splays faults at the northern tip of the Trougout fault are buried under 10-20 ms twtt, which amounts to around 8 m of sediments (Fig. 5). If we consider an average sedimentation rate of 0.2 mm/yr (Martínez-García et al., 2013), there is no record of tectonic activity on these faults since 38ky-77ky, at the scale of the seismic reflection. Our results are in agreement with Poujol et al. (2014) which shows, based on cosmogenic isotopes analysis on the fault mirror of the Trougout fault, indications of a regular decrease of the slip rate on the Trougout fault since the Middle Pleistocene. The connection of F18 and F19 to the Trougout fault show that the recent NW-SE family of normal faults post-dates the N-S Trougout fault, and by extension the regional N-S structures (Fig. 13 and 14B). The change of orientation of the normal faults is compatible with a local counter-clockwise rotation of the stress field (Aït Brahim & Chotin 1990; Palano, et al. 2013) and with the normal-sinistral motion along the Trougout fault onshore (Poujol et al. 2014).

The sub-basin bounded by F18-F19 is wider towards the Trougout fault (Fig. 13 and 14), which suggests however that the normal faults can accommodate part of the recent oblique motion along the offshore/onshore segment of the Trougout fault, despite the lack of recording of onshore activity (e.g. Stich et al. 2005; van der Woerd et al. 2014). We conclude from the interpretation of seismic profiles that there is a continuous present day subsidence in the western part of the basin. The extension seems less active and continuous in the eastern part of the basin, and seems related to the activity of the Trougout fault.

The obliquity of the active NW-SE normal faults in the basin between the northern PDZ and the master faults (i.e. the Trougout fault) clearly demonstrates the transtensional behaviour of the Nekor basin (Fig. 3 and 14) (e.g. Wu et al. 2009). A weak basal detachment level is necessary to create a roll-over structure within the master faults of a pull-apart basin in analogous modelling (e.g. Rahe, et al. 1998; Wu et al. 2009). The asymmetry of the basin is compatible with such roll-over geometry at depth in accordance with a crustal detachment obtained around 9-12km from tomography study from (van der Woerd et al., 2014). The Trougout fault limits this roll-over structure to the east. The extension could be a detachment rooted on an inherited discontinuity in the basement (Galindo-Zaldívar et al. 2009; van der Woerd et al. 2014; d'Acremont et al. 2014), in a way similar to what is observed in the Vienna basin (Fodor 1995; Wu et al. 2009).

The Nekor basin can then be seen as an hybrid transtensional pull-apart basin in the sense of Rahe et al. (1998), with active Quaternary N-S master faults (i.e. the Rouadi and El-Hammam faults to the west and the Trougout-Bou Haddad faults to the East), and oblique NW-SE extensional faults in the basin, likely rooted on a weak level in the basement. As an hybrid pull-apart basin, the concentration of strain along present-day active structures in the western part of the Nekor basin could reflect the asymmetry of the deformation rates between the boundaries of the Nekor basin with its adjacent blocks (the Betico-Rifian and the Nubia blocks, respectively; inset Fig. 14B) (Rahe et al. 1998). The evolution of the depocentres and of the fault activities indicates that the extension in the basin could have migrated from the east to the west and is now localized in the western part of the basin where the earthquakes with the highest magnitude occur. The localisation of the deformation in the Nekor basin and the migration of the deformation could reflect a change in the local kinematic in a Plio-Quaternary continuum of extension.

Present-day kinematic of the Nekor Basin

As a pull-apart basin, the Nekor basin evidences mechanical properties of a transtensive area (Fig. 1B). Recent normal faults can be used to determine the small axis of the stress ellipsoid in a strike–slip context (e.g. Dooley & Schreurs, 2012). If we hypothesize that the family of east and west dipping NW-SE normal faults is a set of quasi-conjugated normal faults in an andersonian stress regime, and that a coulomb failure criteria is assumed, therefore the average directions of horizontal stress are σH=N155°±2 and σh=N65±2° (Fig. 3D).

Most seismological studies proposed that at the scale of the Nekor basin the orientation of the P axis is around N150°±20° (van der Woerd et al. 2014; Medina 1995; Palano, et al. 2013; Ousadou et al. 2014; Stich et al. 2005; Stich et al. 2006; Bezzeghoud & Buforn 1999; Stich, et al. 2010; Calvert et al. 1997; El Alami et al. 1998). From some of those seismological studies σ1 is oriented NNW-SSE and σ3 is oriented NE-SW with a high stress ratio, i.e. the vertical stress tends to be equal to the main horizontal stress (e.g. van der Woerd et al. 2014; Medina 1995; Ousadou et al. 2014). Local stress directions of maximum shortening obtained in the present study are similar and in the error bar with the stress direction previously reported from CMT inversion (e.g. Ousadou et al.

2014) . The offshore Quaternary faults mapped in this study and onshore active faults are probably formed under the same stress azimuths as the ones deduced from CMT inversion.

However, σH goes astray up to 20° of the regional direction of convergence obtained by DeMets, et al. (2010) and Palano et al. (2013) (Fig. 14). This result implies a rotation of the local stress field from the regional convergence. In addition, the angle between the N049° PDZs and the N130° present-day direction of convergence should induce dextral transpression in the Nekor basin (Inset Fig 14B) (Dewey 2002).

We infer that the sinistral transtension deduced from the faults pattern and numerical modelling is compatible with $\sigma 1=\sigma V$, with σH and σh oriented NNW-SSE and NE-SW respectively (Fernández-Ibáñez et al. 2007; Poujol, et al. 2014; Galindo-Zaldívar et al. 2015). Indeed, vertical shortening along the normal fault suggests an elongation of the Nekor basin oriented N245° (inset Fig. 14B). The direction of elongation is compatible with a direction of the minimum horizontal strain parallel to σH (Palano, et al. 2013). The PDZs (Bokkoya-Bousekkour-Aghbal and Nekor fault zones) are inherited from orogenic structures and are reactivated on weak structural discontinuities with a strike–slip style. The orientations of the PDZs with respect to the direction of transport (i.e. the regional convergence or the direction of Rif escape) control the local deformation (Sanderson & Marchini 1984; Teyssier, et al. 1995; Jones, et al. 1997). Our results imply that the Eurasia-Africa convergence alone cannot explain the transtensional behaviour of the Nekor Basin. The transtensional faulting could thus indicate deeper processes in agreement with the Betico-Rifian block direction of transport.

Geodynamic implications

Our data show that the Nekor Basin is located in an area transferring the sinistral displacement along the TASZ to the Rifian Unit (Fig. 14). The pattern above the Bokkoya fault zone, the inactivity of normal faults east of the Trougout fault, as well as the change from distributed normal faulting in the early Pleistocene to localization on a few NW-SE normal faults suggests a change in the local kinematics during the Quaternary. We hypothesize, in accordance with the results of Martínez-García et al. (2013), that a counter-clockwise block rotation along strike-slip faults has led to the formation and propagation of the Al-Idrissi fault toward the south to the Nekor basin. As a result, local change in kinematics in the Nekor basin, together with the activation of the northern PDZ, could reflect the onset of the propagation of the left-lateral TASZ across Rifian alpine structures. The Bokkoya fault is used as a left-lateral transfer fault bounding the Nekor basin to the North. The N-S normal structures are reactivated as normal-dextral and NW-SE normal faulting in the basin becomes dominant.

In western Mediterranean, the geodynamic process is mainly driven by lithospheric scaled processes (e.g. Palano et al. 2013). The slab rollback has moved from the eastern part of the western Mediterranean to end up westward into the Al-Hoceima region (Jolivet et al. 2009; Faccenna et al. 2014). Recent results in tomography have shown that the Alboran sinking slab is detached from the base of the thin crust under the Al Hoceima area and is still likely to be attached to the thick crust under the Rif Mountains westward and southward, thus causing active mantle delamination and crustal thickening (Fig. 1B) (Palomeras et al. 2014; Thurner et al. 2014; Mancilla and Diaz 2015; Petit et al. 2015). As demonstrated by GPS measurements in Vernant et al. (2010), Koulali et al. (2011) and Palano et al. (2013), western Rif Units are moving toward the SW, relative to the Nubia geodetic plate (Fig. 1B). It suggests that the coupling between the Alboran slab and the Rifian crust controls the SW transport direction of the central Rif. Such transport direction fits well with the NE-SW direction of extension deduced in the Nekor basin from the geometry of active normal faulting (Fig. 14). The migration of the deformation toward the west could be related to the progressive westward delamination and rollback of the slab beneath the over-ridding plate. The mantle process (internal dynamics) rather than a large-scale plate convergence, seems to exert a primary role on the surface expression of the active tectonics of the southern margin of the Alboran

Domain, as proposed at the Mediterranean scale by Faccenna et al. 2014. The TASZ highlights however the recent influence of the Africa-Eurasia convergence on the deformation of the over-ridding plate.

Conclusions

New data acquired offshore northern Morocco provide new insights into the Quaternary tectonic evolution of the Nekor basin. We have shown here that:

1. The Nekor basin is a transtensional basin which is rhombohedral in shape. The basin is affected by normal faults that trend N155°. Those normal faults are more recent than the NS fault to which they connect, and they are parallel to the Ajdir-Imzouren fault onshore. The average N31° fault traces on the seafloor define a continuous shear zone which probably connects to the Al-Idrissi fault zone to the north and is the northern PDZ of the Nekor basin. The kinematics of the *en echelon* strike–slip fault zone is sinistral. This shear zone appears to be the trace at the seafloor of a basement fault which runs parallel to the N49° Nekor fault. These structures represent the main displacement zones and the northern and southern boundaries of the Nekor transtensional basin, respectively. These PDZs are parallel to the NW-SE direction of Alpine structures.

2. The geometry of the Nekor basin implies a detachment at the basement level. Consequently, the Nekor basin is likely to be an hybrid basin with master faults that were active in the Quaternary. The migration of the depocentre from the eastern part of the basin westward may reflect the asymmetry of the deformation rates at the boundaries of the Nekor basin, in agreement with the change of direction of GPS vectors at both sides of the basin.

3. The network of N155° normal faults is active, indicating the local direction of the stress (σH=N155°, σh=N065°), and is compatible with the one deduced from local inversion of moment tensors. It suggests that there is no short-term rotation of the stress field. The transtensional pattern

indicates vertical shortening of the Nekor basin. The transtension and the NE-SW orientation of the PDZ are not compatible with the regional direction of convergence. NE-SW faults post-date the N-S Trougout fault. The Nekor basin appears to have undergone counter-clockwise rotation of the stress direction between 0.79Ma and the present period. The active roll-back and detachment of a part of the Tethyan slab at the Al Hoceima region in an orogenic back-arc context could explain the active subsidence and the transtensive tectonics in the Nekor basin. Mantle dynamics, more than the Africa-Eurasia convergence, appears to be the main control of the transtensional surface deformation in the over-ridding plate at the southern margin of the Alboran Domain.

ACKNOWLEDGEMENTS

We thank G. Ercilla, B. El Moumni and A. Benjouad for affirmative help to the program; the Moroccan authorities and ANCFCC for the GPS data, and DPDPM for the tide-gauge data. The CNRS-INSU provided marine facilities. This work was funded by the French program Actions Marges, the LabexMER "Investment for the future" (ANR-10-LABX-19-01), the EUROFLEETS program (FP7/2007-2013; n°228344), project FICTS-2011-03-01. The processed seismic data were interpreted thanks to the Kingdom Suite©software. We thank the editor C. Ebinger, and the reviewers S. Ceramicola, M.-A. Gutscher and an anonymous reviewer who helped us to enhance the quality of this article.

Conflict of interest

No conflict of interest declared

Reference List

Aït Brahim, L. (1985) Migration Des Aires De Subsidence Maximum Et Réorientation De La Direction Du Champ De Contrainte Dans Les Bassins Néogènes Du Maroc Septentrional. *Bulletin de l'Institut Scientifique, Rabat*, **9,** 89-96.

Aït Brahim, L. & Chotin, P. (1990) Oriental Moroccan Neogene Volcanism and Strike-Slip Faulting. *Journal of African Earth Sciences*, **11,** 273-280.

Aït Brahim, L., Tadili, B., Nakhcha, C., Mouayn, I., Ramdani, M., Limouri, M., El Qadi, A., Sossey Alaoui, F. & Benhalima, M. (2004) Using Active Faults and Seismicity for the Strong Motion Modeling in the Eastern Rif (Northern Morocco). *Pure and*

Applied Geophysics, **161,** 1081-1091.

Akoglu, A.M., Cakir, Z., Meghraoui, M., Belabbes, S., El Alami, S., Ergintav, S. & Akyüz, H.S. (2006) The 1994–2004 Al Hoceima (Morocco) Earthquake Sequence: Conjugate Fault Ruptures Deduced from Insar. *Earth and Planetary Science Letters*, **252,** 467-480.

Allen, M.B., Macdonald, D.I.M., Xun, Z., Vincent, S.J. & Brouet-Menzies, C. (1998) Transtensional Deformation in the Evolution of the Bohai Basin, Northern China. *Geological Society, London, Special Publications*, **135,** 215-229.

Allmendinger, R.W., Jordan, T.E., Kay, S.M. & Isacks, B.L. (1997) The Evolution of the Altiplano-Puna Plateau of the Central Andes. *Annual Review of Earth and Planetary Sciences*, **25,** 139-174.

Allmendinger, R.W., Cardozo, N.C. & Fisher, D. (2012) *Structural Geology Algorithms: Vectors & Tensors*. Cambridge University Press, Cambridge, England.

Ammar, A., Mauffret, A., Gorini, C. & Jabour, H. (2007) The Tectonic Structure of the Alboran Margin of Morocco. *Revista de la Sociedad Geológica de España*, **20,** 247–271.

Asebriy, L., Luca, P., Bourgois, J. & Chotin, P. (1987) Resédimentations D'âge Sénonien Dans Le Rif Central (Maroc): Conséquences Sur Les Divisions Paléogéographiques Et Structurales De La Chaîne. *Journal of African Earth Sciences (1983)*, **6,** 9–17.

Asebriy, L., Bourgois, J., Cherkaoui, T.E. & Azdimousa, A. (1993) Evolution Tectonique Récente De La Zone De Faille Du Nékor: Importance Paléogéographique Et Structurale Dans Le Rif Externe, Maroc. *Journal of African Earth Sciences (and the Middle East)*, **17,** 65–74.

Ballesteros, M., Rivera, J., Muñoz, A., Muñoz-Martín, A., Acosta, J., Carbó, A. & Uchupi, E. (2008) Alboran Basin, Southern Spain—Part Ii: Neogene Tectonic Implications for the Orogenic Float Model. *Marine and Petroleum Geology*, **25,** 75-101.

Barnes, P.M. & Pondard, N. (2010) Derivation of Direct on-Fault Submarine Paleoearthquake Records from High-Resolution Seismic Reflection Profiles: Wairau Fault, New Zealand: Submarine Paleoearthquake Records. *Geochemistry, Geophysics, Geosystems*, **11,** n/a-n/a.

Benzaggagh, M., Mokhtari, A., Rossi, P., Michard, A., El Maz, A., Chalouan, A., Saddiqi, O. & Rjimati, E.-C. (2014) Oceanic Units in the Core of the External Rif (Morocco): Intramargin Hiatus or South-Tethyan Remnants? *Journal of Geodynamics*, **77,** 4-21.

Bezzeghoud, M. & Buforn, E. (1999) Source Parameters of the 1992 Melilla (Spain, Mw= 4.8), 1994 Alhoceima (Morocco, Mw= 5.8), and 1994 Mascara (Algeria, Mw= 5.7) Earthquakes and Seismotectonic Implications. *Bulletin of the Seismological Society of America*, **89,** 359–372.

Biggs, J., Bergman, E., Emmerson, B., Funning, G.J., Jackson, J., Parsons, B. & Wright, T.J. (2006) Fault Identification for Buried Strike-Slip Earthquakes Using Insar: The 1994 and 2004 Al Hoceima, Morocco Earthquakes. *Geophysical Journal International*, **166,** 1347-1362.

Bird, P. (2003) An Updated Digital Model of Plate Boundaries. *Geochem. Geophys. Geosyst.*, **4,** 1027.

Bourgois, J., Mauffret, A., Ammar, A. & Demnati, A. (1992) Multichannel Seismic Data Imaging of Inversion Tectonics of the Alboran Ridge (Western Mediterranean Sea). *Geo-Marine Letters*, **12,** 117–122.

Cakir, Z., Meghraoui, M., Akoglu, A.M., Jabour, N., Belabbes, S. & Ait-Brahim, L. (2006) Surface Deformation Associated with the Mw 6.4, 24 February 2004 Al Hoceima, Morocco, Earthquake Deduced from Insar: Implications for the Active Tectonics Along North Africa. *Bulletin of the Seismological Society of America*, **96,** 59-68.

Calais, E., DeMets, C. & Nocquet, J.-M. (2003) Evidence for a Post-3.16-Ma Change in Nubia–Eurasia–North America Plate Motions? *Earth and Planetary Science Letters*, **216,** 81-92.

Calvert, A., Gomez, F., Seber, D., Barazangi, M., Jabour, N., Ibenbrahim, A. & Demnati, A. (1997) An Integrated Geophysical Investigation of Recent Seismicity in the Al-Hoceima Region of North Morocco. *Bulletin of the Seismological Society of America*, **87,** 637–651.

Calvert, A., Sandvol, E., Seber, D., Barazangi, M., Roecker, S., Mourabit, T., Vidal, F., Alguacil, G. & Jabour, N. (2000) Geodynamic Evolution of the Lithosphere and Upper Mantle beneath the Alboran Region of the Western Mediterranean: Constraints from Travel Time Tomography. *Journal of Geophysical Research: Solid Earth*, **105,** 10871-10898.

Campillo, A.C., Maldonado, A. & Mauffret, A. (1992) Stratigraphic and Tectonic Evolution of the Western Alboran Sea: Late Miocene to Recent. *Geo-Marine Letters*, **12,** 165–172.

Cardozo, N. & Allmendinger, R.W. (2013) Spherical Projections with Osxstereonet: Computers & Geosciences. **51,** 193 - 205.

Chalouan, A., Michard & A. (2004) The Alpine Rif Belt (Morocco): A Case of Mountain Building in a Subduction-Subduction-Transform Fault Triple Junction. *Pure and Applied Geophysics*, **161,** 489–519.

Chalouan, A., Michard, A., EL KADIRI, K., Negro, F., Frizon de Lamotte, D., Soto, J.I. & Saddiqi, O. (2008) The Rif Belt. In: *Continental Evolution: The Geology of Morocco* (Ed. by, 203-302.

Comas, M.C., Platt, J.P., Soto, J.I. & Watts, A.B. (1999) The Origin and Tectonic History of the Alboran Basin: Insights from Leg 161 Results. *Proceedings of the Ocean Drilling Program Scientific Results*, **161,** 555–580.

Cunha, T.A., Matias, L.M., Terrinha, P., Negredo, A.M., Rosas, F., Fernandes, R.M.S. & Pinheiro, L.M. (2012) Neotectonics of the Sw Iberia Margin, Gulf of Cadiz and Alboran Sea: A Reassessment Including Recent Structural, Seismic and Geodetic

Data: Neotectonics Sw Iberia-Gulf of Cadiz-Alboran. *Geophysical Journal International*, **188,** 850-872.

Curren, I.S. & Bird, P. (2014) Formation and Suppression of Strike–Slip Fault Systems. *Pure and Applied Geophysics*.

d'Acremont, E., Alonso, B., Ercilla, G. & Vandorpe, T. (2013). *Active Sedimentation and Tectonics in the South Alboran Sea: Preliminary Results of the Marlboro and Saras Surveys*.

d'Acremont, E., Gutscher, M.-A., Rabaute, A., Mercier de Lépinay, B., Lafosse, M., Poort, J., Ammar, A., Tahayt, A., Le Roy, P., Smit, J., Do Couto, D., Cancouët, R., Prunier, C., Ercilla, G. & Gorini, C. (2014) High-Resolution Imagery of Active Faulting Offshore Al Hoceima, Northern Morocco. *Tectonophysics*.

De Larouzière, F.D., Bolze, J., Bordet, P., Hernandez, J., Montenat, C. & Ott d'Estevou, P. (1988) The Betic Segment of the Lithospheric Trans-Alboran Shear Zone During the Late Miocene. *Tectonophysics*, **152,** 41-52.

De Vicente, G., Giner, J.L., Muñoz-Martín, A., González-Casado, J.M. & Lindo, R. (1996) Determination of Present-Day Stress Tensor and Neotectonic Interval in the Spanish Central System and Madrid Basin, Central Spain. *Tectonophysics*, **266,** 405-424.

Decker, K., Peresson, H. & Hinsch, R. (2005) Active Tectonics and Quaternary Basin Formation Along the Vienna Basin Transform Fault. *Quaternary Science Reviews*, **24,** 305-320.

DeMets, C., Gordon, R.G. & Argus, D.F. (2010) Geologically Current Plate Motions. *Geophysical Journal International*, **181,** 1-80.

Dewey, J.F., Holdsworth, R.E. & Strachan, R.A. (1998) Transpression and Transtension Zones. *Geological Society, London, Special Publications*, **135,** 1-14.

Dooley, T.P. & Schreurs, G. (2012) Analogue Modelling of Intraplate Strike-Slip Tectonics: A Review and New Experimental Results. *Tectonophysics*, **574-575,** 1-71.

Duggen, S., Hoernle, K., van den Bogaard, P. & Harris, C. (2004) Magmatic Evolution of the Alboran Region: The Role of Subduction in Forming the Western Mediterranean and Causing the Messinian Salinity Crisis. *Earth and Planetary Science Letters*, **218,** 91-108.

El Alami, S.O., Tadili, B.A., Cherkaoui, T.E., Medina, F., Ramdani, M., Brahim, L.A. & Harnafi, M. (1998) The Al Hoceima Earthquake of May 26, 1994 and Its Aftershocks: A Seismotectonic Study. *ANALI DI GEOFISICA*, **41,** 519-537.

El Azzouzi, M., Bellon, H., Coutelle, A. & Réhault, J.-P. (2014) Miocene Magmatism and Tectonics within the Peri-Alboran Orogen (Western Mediterranean). *Journal of Geodynamics*, **77,** 171-185.

Estrada, F., Vazquez, J.T., Ercilla, G., Alonso, B., d'Acremont, E., Gorini, C., Gomez, M., Fernandez-Puga, M.C., Ammar, A. & El Moumni, B. (2014) Recent Tectonic Inversion of the Central Alboran Zone. *Resúmenes de la 2ª Reunión Ibérica sobre Fallas Activas y Paleosismología***,** 51.

Faccenna, C., Becker, T.W., Auer, L., Billi, A., Boschi, L., Brun, J.P., Capitanio, F.A., Funiciello, F., Horvàth, F. & Jolivet, L. (2014) Mantle Dynamics in the Mediterranean. *Reviews of Geophysics*, **52,** 283-332.

Fadil, A., Vernant, P., McClusky, S., Reilinger, R., Gomez, F., Ben Sari, D., Mourabit, T., Feigl, K. & Barazangi, M. (2006) Active Tectonics of the Western Mediterranean: Geodetic Evidence for Rollback of a Delaminated Subcontinental Lithospheric Slab beneath the Rif Mountains, Morocco. *Geology*, **34,** 529.

Fernández-Ibáñez, F., Soto, J.I., Zoback, M.D. & Morales, J. (2007) Present-Day Stress Field in the Gibraltar Arc (Western Mediterranean). *Journal of Geophysical Research*, **112**.

Fodor, L. (1995) From Transpression to Transtension: Oligocene-Miocene Structural Evolution of the Vienna Basin and the East Alpine-Western Carpathian Junction. *Tectonophysics*, **242,** 151-182.

Galindo-Zaldívar, J., González-Lodeiro, F. & Jabaloy, A. (1993) Stress and Palaeostress in the Betic-Rif Cordilleras (Miocene to the Present). *Tectonophysics*, **227,** 105-126.

Galindo-Zaldívar, J., Chalouan, A., Azzouz, O., Sanz de Galdeano, C., Anahnah, F., Ameza, L., Ruano, P., Pedrera, A., Ruiz-Constán, A., Marín-Lechado, C., Benmakhlouf, M., López-Garrido, A.C., Ahmamou, M., Saji, R., Roldán-García, F.J., Akil, M. & Chabli, A. (2009) Are the Seismological and Geological Observations of the Al Hoceima (Morocco, Rif) 2004 Earthquake (M=6.3) Contradictory? *Tectonophysics*, **475,** 59-67.

Galindo-Zaldívar, J., Azzouz, O., Chalouan, A., Pedrera, A., Ruano, P., Ruiz-Constán, A., Sanz de Galdeano, C., Marín-Lechado, C., López-Garrido, A.C., Anahnah, F. & Benmakhlouf, M. (2015) Extensional Tectonics, Graben Development and Fault Terminations in the Eastern Rif (Bokoya–Ras Afraou Area). *Tectonophysics*.

Gràcia, E., Pallàs, R., Soto, J.I., Comas, M., Moreno, X., Masana, E., Santanach, P., Diez, S., García, M. & Dañobeitia, J. (2006) Active Faulting Offshore Se Spain (Alboran Sea): Implications for Earthquake Hazard Assessment in the Southern Iberian Margin. *Earth and Planetary Science Letters*, **241,** 734-749.

Gutscher, M.-A., Malod, J., Rehault, J.-P., Contrucci, I., Klingelhoefer, F., Mendes-Victor, L. & Spakman, W. (2002) Evidence for Active Subduction beneath Gibraltar. *Geology*, **30,** 1071-1074.

Gutscher & A., M. (2004) What Caused the Great Lisbon Earthquake? *Science*, **305,** 1247–1248.

Harris, R.A. & Day, S.M. (1993) Dynamics of Fault Interaction: Parallel Strike-Slip Faults. *Journal of Geophysical Research: Solid Earth*, **98,** 4461-4472.

Hatzfeld, D., Caillot, V., Cherkaoui, T.-E., Jebli, H. & Medina (1993) Microearthquake Seismicity and Fault Plane Solutions around the Nékor Strike-Slip Fault, Morocco. *Earth and Planetary Science Letters*.

Herraiz, M., De Vicente, G., Lindo-Ñaupari, R., Giner, J., Simón, J.L., González-Casado, J.M., Vadillo, O., Rodríguez-Pascua, M.A., Cicuéndez, J.I., Casas, A., Cabañas, L., Rincón, P., Cortés, A.L., Ramírez, M. & Lucini, M. (2000) The Recent (Upper Miocene to Quaternary) and Present Tectonic Stress Distributions in the Iberian Peninsula. *Tectonics*, **19,** 762-786.

Hölzel, M., Decker, K., Zámolyi, A., Strauss, P. & Wagreich, M. (2010) Lower Miocene Structural Evolution of the Central Vienna Basin (Austria). *Marine and Petroleum Geology*, **27,** 666-681.

Jabour, N., Kasmi, M., Menzhi, M., Birouk, A., Hni, L., Hahou, Y., Timoulali, Y. & Badrane, S. (2004) The February 24th, 2004 Al Hoceima Earthquake. *CSEM-EMSC (www. emsc-csem. org), Newsletter*.

Jolivet, L., Augier, R., Faccenna, C., Negro, F., Rimmele, G., Agard, P., Robin, C., Rossetti, F. & Crespo-Blanc, A. (2008) Subduction, Convergence and the Mode of Backarc Extension in the Mediterranean Region. *Bulletin de la Société Géologique de France*, **179,** 525–550.

Jolivet, L., Faccenna, C., Piromallo & C. (2009) From Mantle to Crust: Stretching the Mediterranean. *Earth and Planetary Science Letters*, **285,** 198–209.

Jones, R.R., Holdsworth, R.E. & Bailey, W. (1997) Lateral Extrusion in Transpression Zones: The Importance of Boundary Conditions. *Journal of Structural Geology*, **19,** 1201-1217.

Koulali, A., Ouazar, D., Tahayt, A., King, R.W., Vernant, P., Reilinger, R.E., McClusky, S., Mourabit, T., Davila, J.M. & Amraoui, N. (2011) New Gps Constraints on Active Deformation Along the Africa–Iberia Plate Boundary. *Earth and Planetary Science Letters*, **308,** 211-217.

Leblanc, D. & Olivier, P. (1984) Role of Strike-Slip Faults in the Betic-Rifian Orogeny. *Tectonophysics*, **101,** 345-355.

Levander, A., Bezada, M.J., Niu, F., Humphreys, E.D., Palomeras, I., Thurner, S.M., Masy, J., Schmitz, M., Gallart, J., Carbonell, R. & Miller, M.S. (2014) Subduction-Driven Recycling of Continental Margin Lithosphere. *Nature*, **515,** 253-256.

Lobo, F.J. & Ridente, D. (2014) Stratigraphic Architecture and Spatio-Temporal Variability of High-Frequency (Milankovitch) Depositional Cycles on Modern Continental Margins: An Overview. *Marine Geology*, **352,** 215-247.

Lonergan, L. & White, N. (1997) Origin of the Betic-Rif Mountain Belt. *Tectonics*, **16,** 504-522.

Mancilla, F.d.L. & Diaz, J. High Resolution Moho Topography Map beneath Iberia and Northern Morocco from Receiver Function Analysis. *Tectonophysics*.

Mann, P. (2007) Global Catalogue, Classification and Tectonic Origins of Restraining- and Releasing Bends on Active and Ancient Strike-Slip Fault Systems. *Geological Society, London, Special Publications*, **290,** 13-142.

Martínez-García, P., Soto, J.I. & Comas, M. (2011) Recent Structures in the Alboran Ridge and Yusuf Fault Zones Based on Swath Bathymetry and Sub-Bottom Profiling: Evidence of Active Tectonics. *Geo-Marine Letters*, **31,** 19-36.

Martínez-García, P., Comas, M., Soto, J.I., Lonergan, L. & Watts, A.B. (2013) Strike-Slip Tectonics and Basin Inversion in the Western Mediterranean: The Post-Messinian Evolution of the Alboran Sea. *Basin Research*, **25,** 361-387.

Mauffret, A., Maldonado, A. & Campillo, A.C. (1992) Tectonic Framework of the Eastern Alboran and Western Algerian Basins, Western Mediterranean. *Geo-Marine Letters*, **12,** 104–110.

McClay, K. & Dooley, T. (1995) Analogue Models of Pull-Apart Basins. *Geology*, **23,** 711–714.

Medina, F. (1995) Present-Day State of Stress in Northern Morocco from Focal Mechanism Analysis. *Journal of Structural Geology*, **17,** 1035-1046.

Medina, F. & El Alami, S.O. (2006) Focal Mechanisms and State of Stress in the Al Hoceima Area (Central Rif, Morocco). *Bull Inst Sci, Rabat, sect Sci Terre*, **28,** 19–30.

Michard, A., Feinberg, H., El-Azzab, D., Bouybaouene, M. & Saddiqi, O. (1992) A Serpentinite Ridge in a Collisional Paleomargin Setting: The Beni Malek Massif, External Rif, Morocco. *Earth and planetary science letters*, **113,** 435–442.

Michard, A., Negro, F., de Lamotte, D.F. & Saddiqi, O. (2007) Serpentinite Slivers and Metamorphism in the External Maghrebides: Arguments for an Intracontinental Suture in the African Paleomargin (Morocco, Algeria). *Revista de la Sociedad Geológica de España*, **20,** 173–186.

Morel, J.-L. (1988) *Evolution Récente De L'orogène Rifain Et De Son Avant-Pays Depuis La Fin De La Mise En Place Des Nappes (Rif, Maroc)*. Géodiffusion éd.

Morel, J.-L. & Meghraoui, M. (1996) Goringe-Alboran-Tell Tectonic Zone: A Transpression System Along the Africa-Eurasia Plate Boundary. *Geology*, **24,** 755–758.

Nash, D. (2013) Tectonic Geomorphology of Normal Fault Scarps. In: *Treatise on Geomorphology* (Ed. by J. F. Shroder), 234-249. Academic Press, San Diego.

Naylor, M.A., Mandl, G. & Supesteijn, C.H.K. (1986) Fault Geometries in Basement-Induced Wrench Faulting under Different Initial Stress States. *Journal of Structural Geology*, **8,** 737-752.

Negredo, A.M. (2002) Neotectonic Modeling of the Ibero-Maghrebian Region. *Journal of Geophysical Research*, **107**.

Negro, F., Agard, P., Goffe, B. & Saddiqi, O. (2007) Tectonic and Metamorphic Evolution of the Temsamane Units, External Rif (Northern Morocco): Implications for the Evolution of the Rif and the Betic-Rif Arc. *Journal of the Geological Society*, **164,** 829-842.

Nocquet, J.-M. (2012) Present-Day Kinematics of the Mediterranean: A Comprehensive Overview of Gps Results.

Tectonophysics, **579,** 220-242.

Ousadou, F., Dorbath, L., Ayadi, A., Dorbath, C. & Gharbi, S. (2014) Stress Field Variations Along the Maghreb Region Derived from Inversion of Major Seismic Crisis Fault Plane Solutions. *Tectonophysics*, **632,** 261-280.

Palano, M., González, P.J. & Fernández, J. (2013) Strain and Stress Fields Along the Gibraltar Orogenic Arc: Constraints on Active Geodynamics. *Gondwana Research*, **23,** 1071-1088.

Palomeras, I., Thurner, S., Levander, A., Liu, K., Villasenor, A., Carbonell, R. & Harnafi, M. (2014) Finite-Frequency Rayleigh Wave Tomography of the Western Mediterranean: Mapping Its Lithospheric Structure: Rayleigh Wave Vs Model in Wm. *Geochemistry, Geophysics, Geosystems*, **15,** 140-160.

Pedrera, A., Ruiz-Constán, A., Galindo-Zaldívar, J., Chalouan, A., Sanz de Galdeano, C., Marín-Lechado, C., Ruano, P., Benmakhlouf, M., Akil, M., López-Garrido, A.C., Chabli, A., Ahmamou, M. & González-Castillo, L. (2011) Is There an Active Subduction beneath the Gibraltar Orogenic Arc? Constraints from Pliocene to Present-Day Stress Field. *Journal of Geodynamics*, **52,** 83-96.

Perouse, E., Vernant, P., Chery, J., Reilinger, R. & McClusky, S. (2010) Active Surface Deformation and Sub-Lithospheric Processes in the Western Mediterranean Constrained by Numerical Models. *Geology*, **38,** 823-826.

Petit, C., Pourhiet, L.L., Scalabrino, B., Corsini, M., Bonnin, M. & Romagny, A. (2015) Crustal Structure and Gravity Anomalies beneath the Rif, Northern Morocco: Implications for the Current Tectonics of the Alboran Region. *Geophysical Journal International*, **202,** 640-652.

Platt, J.P., Soto, J.-I., Whitehouse, M.J., Hurford, A.J. & Kelley, S.P. (1998) Thermal Evolution, Rate of Exhumation, and Tectonic Significance of Metamorphic Rocks from the Floor of the Alboran Extensional Basin, Western Mediterranean. *Tectonics*, **17,** 671-689.

Poujol, A., Ritz, J.-F., Tahayt, A., Vernant, P., Condomines, M., Blard, P.-H., Billant, J., Vacher, L., Tibari, B., Hni, L. & Koulali, A. (2014) Active Tectonics of the Northern Rif (Morocco) from Geomorphic and Geochronological Data. *Journal of Geodynamics*, **77,** 70-88.

Rabineau, M., Berné, S., Aslanian, D., Olivet, J.-L., Joseph, P., Guillocheau, F., Bourillet, J.-F., Ledrezen, E. & Granjeon, D. (2005) Sedimentary Sequences in the Gulf of Lion: A Record of 100,000 Years Climatic Cycles. *Marine and Petroleum Geology*, **22,** 775-804.

Rahe, B., Ferrill, D.A. & Morris, A.P. (1998) Physical Analog Modeling of Pull-Apart Basin Evolution. *Tectonophysics*, **285,** 21–40.

Ratschbacher, L., Frisch, W., Linzer, H.-G. & Merle, O. (1991) Lateral Extrusion in the Eastern Alps, Part 2: Structural Analysis. *Tectonics*, **10,** 257-271.

Richard, P.D., Naylor, M.A. & Koopman, A. (1995) Experimental Models of Strike-Slip Tectonics. *Petroleum Geoscience*, **1,** 71–80.

Rodriguez, M., Chamot-Rooke, N., Fournier, M., Huchon, P. & Delescluse, M. (2013) Mode of Opening of an Oceanic Pull-Apart: The 20°N Basin Along the Owen Fracture Zone (Nw Indian Ocean): Opening of the 20°N Pull-Apart Basin. *Tectonics*, **32,** 1343-1357.

Sanderson, D.J. & Marchini, W.R.D. (1984) Transpression. *Journal of Structural Geology*, **6,** 449-458.

Seber, D., Barazangi, M., Ibenbrahim, A. & Demnati, A. (1996) Geophysical Evidence for Lithospheric Delamination beneath the Alboran Sea and Rif–Betic Mountains. *Nature*, **379,** 785-790.

Stich, D., Ammon, C. & Morales, J. (2003) Moment Tensor Solutions for Small and Moderate Earthquakes in the Ibero-Maghreb Region. *Journal of Geophysical Research*, **108**.

Stich, D., Mancilla, F.d.L., Baumont, D. & Morales, J. (2005) Source Analysis of the Mw 6.3 2004 Al Hoceima Earthquake (Morocco) Using Regional Apparent Source Time Functions. *Journal of Geophysical Research*, **110**.

Stich, D., Serpelloni, E., de Lis Mancilla, F. & Morales, J. (2006) Kinematics of the Iberia–Maghreb Plate Contact from Seismic Moment Tensors and Gps Observations. *Tectonophysics*, **426,** 295-317.

Stich, D., Martín, R. & Morales, J. (2010) Moment Tensor Inversion for Iberia–Maghreb Earthquakes 2005–2008. *Tectonophysics*, **483,** 390-398.

Tahayt, A., Mourabit, T., Rigo, A., Feigl, K.L., Fadil, A., McClusky, S., Reilinger, R., Serroukh, M., Ouazzani-Touhami, A., Sari, D.B. & Vernant, P. (2008) Mouvements Actuels Des Blocs Tectoniques Dans L'arc Bético-Rifain À Partir Des Mesures Gps Entre 1999 Et 2005. *Comptes Rendus Geoscience*, **340,** 400–413.

Tahayt, A., Feigl, K.L., Mourabit, T., Rigo, A., Reilinger, R., McClusky, S., Fadil, A., Berthier, E., Dorbath, L., Serroukh, M., Gomez, F. & Ben Sari, D. (2009) The Al Hoceima (Morocco) Earthquake of 24 February 2004, Analysis and Interpretation of Data from Envisat Asar and Spot5 Validated by Ground-Based Observations. *Remote Sensing of Environment*, **113,** 306-316.

Taymaz, T., Jackson, J. & McKenzie, D. (1991) Active Tectonics of the North and Central Aegean Sea. *Geophysical Journal International*, **106,** 433-490.

Tesson, M., Gensous, B. & Labraimi, L. (1987) Seismic Analysis of the Southern Margin of the Alboran Sea. *Journal of African Earth Sciences*, **6,** 813–821.

Tesson, M. & Gensous, B. (1989) Les Bases D'une Stratigraphie Sismique Du Néogène Post-Nappes En Mer D'alboran, Au Large Du Maroc. Implications Structurales Et Paléogéographiques. *Journal of African Earth Sciences (and the Middle East)*, **9,** 421-433.

Teyssier, C., Tikoff, B. & Markley, M. (1995) Oblique Plate Motion and Continental Tectonics. *Geology*, **23,** 447–450.

Thurner, S., Palomeras, I., Levander, A., Carbonell, R. & Lee, C.-T. (2014) Ongoing Lithospheric Removal in the Western Mediterranean: Evidence from Ps Receiver Functions and Thermobarometry of Neogene Basalts (Picasso Project). *Geochemistry, Geophysics, Geosystems*, **15,** 1113-1127.

Van der Woerd, J., Dorbath, C., Ousadou, F., Dorbath, L., Delouis, B., Jacques, E., Tapponnier, P., Hahou, Y., Menzhi, M., Frogneux, M. & Haessler, H. (2014) The Al Hoceima Mw 6.4 Earthquake of 24 February 2004 and Its Aftershocks Sequence. *Journal of Geodynamics*, **77,** 89-109.

Vázquez, J.T., Estrada, F., Vegas, R., Ercilla, G., d'Acremont, E., Fernández-Salas, L.M. & Alonso, B. (2014) Quaternary Tectonics Influence Onthe Adra Continental Slope Morphology (Northern Alboran Sea).

Vernant, P., Fadil, A., Mourabit, T., Ouazar, D., Koulali, A., Davila, J.M., Garate, J., McClusky, S. & Reilinger, R. (2010) Geodetic Constraints on Active Tectonics of the Western Mediterranean: Implications for the Kinematics and Dynamics of the Nubia-Eurasia Plate Boundary Zone. *Journal of Geodynamics*, **49,** 123-129.

Wilcox, R.E., Harding, T.t. & Seely, D.R. (1973) Basic Wrench Tectonics. *AAPG Bulletin*, **57,** 74–96.

Woodside, J.M. & Maldonado, A. (1992) Styles of Compressional Neotectonics in the Eastern Alboran Sea. *Geo-Marine Letters*, **12,** 111–116.

Wu, J.E., McClay, K., Whitehouse, P. & Dooley, T. (2009) 4d Analogue Modelling of Transtensional Pull-Apart Basins. *Marine and Petroleum Geology*, **26,** 1608-1623.

Zecchin, M., Ceramicola, S., Lodolo, E., Casalbore, D. & Chiocci, F.L. (2015) Episodic, Rapid Sea-Level Rises on the Central Mediterranean Shelves after the Last Glacial Maximum: A Review. *Marine Geology*, **369,** 212-223.

Figure captions

Figure 1. A. Structural map of the Rif onshore and of the Alboran basin offshore modified after Chalouan et al. (2008), Martínez-García et al.(2011), Martínez-García et al. (2013), and Ballesteros et al. (2008). A.f.z., Adra fault zone, A-I.f., Al Idrissi fault; A.R., Alboran Ridge, C., Carboneras fault, SAB, South Alboran Basin; T.B. Tofiño Bank. WAB, western Alboran basin; XB, Xauen bank. **B.** Kinematics of the Alboran from GPS data (Koulali et al. 2011), associated with the seismicity between 1964 and 2012 (Spanish Instituto Geografico Nacional (IGN) database) and with the thickness of the crust from receiver function redrawn from Mancilla & Diaz 2015; Red arrow, direction of convergence at the rigid block boundaries (Nocquet 2012). **C**. Regional map of the recent active structures, and shaded relief from the Advanced Spaceborne Thermal Emission and Reflection Radiometer (ASTER) digital elevation model. Swath bathymetry from SARAS and Marlboro-2 cruises (d'Acremont et al. 2014). Focal mechanisms of the 1994 main shock (red star ; El Alami et al. 1998; Biggs et al. 2006) and of the 2004 main shock in violet (van der Woerd et al. 2004). CMT catalog from Bezzeghoud and Buforn (1999). Ras=Cape; A.f., Ajdir fault; B.H.f., Bou Haddad fault; R.f., Rouadi fault, B.f, Bokkoya fault, B.-A.f., Bousekkour-Aghbal fault, I.f., Imzouren fault; T.f., Trougout fault; A.I.f., Al-Idrissi fault; N.f., Nekor fault, E-H.f., El-Hammam fault; N.b., Nekor basin; B.b., Boudinar basin. After Aït Brahim et al. (2004), Medina (1995), Calvert et al. (1997), El Alami et al. (1998), Medina & El Alami (2006), and van der Woerd et al. (2014). The thick crust under the Rifian orogenic arc corresponds approximatively to the area of coupling between the Alboran slab and the Rifian crust (e.g. Perouse et al. 2010; Thurner et al. 2014).

Figure 2. A. Map of the seismic surveys tracklines. Thick line: seismic profiles shown in this studies. Dashed rectangles correspond to focuses on the bathymetry shown in this study. **B&C** Extract of all of the east (blue dots) and west (red dots) dipping faults spottedon the seismic profiles. Thick lines: interpreted fault traces. The black dots in the insert B show the west dipping faults and conversely the black dots in the insert C show the east dipping faults.

Figure 3. A. Interpreted structural map of the study area overimposed on the shaded bathymetry. **B.** Lower-sphere stereographic projection of the fault dataset. **C.** Rose diagram of the fault azimuths. **D.** Kamb contouring of the complete fault dataset. N = 193; contour interval = x2σ; counting area = 0.17 of the net area; significance level = x3σ; σ is the standard deviation. **E.** Kamb contouring of the poles of the normal faults. Stereographic projections of equal area. N = 121; contour interval = x2σ; counting area = 0.17 of the net area; significance level = x3σ. Designed with the help of Stereonet 8 (Allmendinger et al., 2012; Cardozo & Allmendinger, 2013). σ_h: minimum horizontal stress direction. The red area indicates two standard deviations of poles azimuts.

Figure 4. MAB258 seismic reflection profile from the Marlboro-2 survey. Green arrows, toplap; orange reflector, unconformity surface dated around 0.79My. Vertical exaggeration = 10. U1, U2, U3: formations defined from acoustic facies (see main text).

Figure 5. MAB291 seismic reflection profile from the Marlboro-2 survey. Green reflector, erosive surface. Note the truncated faults on the eastern part of the basin. Note the west-dipping fault A which bounds the east of the depocentre above the green surface. Vertical exaggeration: 10. green reflector : top of the pre-extension formation.

Figure 6: A. MAB273 seismic profile. **B.** MAB12 seismic profile. Yellow dashed line: top of the acoustic basement; thin red line: non-outcropping faults; thick red line, outcropping fault; red arrows, onlap termination and syn-sedimentary deposits during the growth of the fold; F, fault. The shallow seafloor prevents the imaging of the deeper part of the basin. White transparent mask, multiples; F1 and F2, fault number (see fig. 11). yellow reflector, top of the pre-extension formation; **Insets:** Position of the seismic profiles on a synthetic map; vertical scale using a velocity of P-waves values equals to 1510m/s. Vertical exaggeration = 10 for the sea-bottom, assuming Vp in water = 1510 m/s.

Figure 7. Seismic reflection profiles MAB29 and MAB33 from the Marlboro-2 survey. Thick red lines, major faults at the basin scale; thin red lines, secondary faults; red arrows, apparent vertical motion along fault planes; yellow reflector, top of the pre-extension formation; shaded area, first multiples. F3 to F8, fault number (see fig. 12). Vertical exaggeration = 10.

Figure 8. A. MAB65 uninterpreted seismic reflexion profile from the Marlboro-2 survey. Vertical exaggeration: 10. **B**. Line-drawing of the MAB65 profile. Small arrows, multiple discordances inside the sedimentary record. Faults: same as for Figure 12.

Figure 9. MAB281 seismic reflection profile from the Marlboro-2 survey. Vertical exaggeration = 9.5; blue line, bottom of the incised paleo-channels; red arrows, onlap; yellow arrows, downlap.

Figure 10. A. TOPAS profile 4242 from the SARAS survey. **B.** Line drawing of TOPAS profile 4242. Vertical exaggeration = 21; M, Seafloor first multiple. Inset: Topography along the A-A' transect. See fig. 12 for location of F15 to F17. **C.** IZD29 profile, modified after Calvert et al. (1997). Dashed purple reflector, bottom reflector of the basin; dashed green reflector, first multiple of the seafloor; red line, faults affecting the bottom reflector of the basin in the Nekor basin; black lines, faults with no imprint on the bathymetry. The position of the TOPAS4242 seismic profile is approximatively projected on the IZD29 seismic profile.

Figure **11:** Shaded relief bathymetric map showing the continuity of the Bousekkour-Aghbal fault. F1, F2, faults; PSL, paleo-shoreline; T, terrace; SB, shelf break; dark orange lines, positions of the seismic profiles (see Fig. 2); black lines, isobaths. The purple line indicates the -125m isobath. The numbering of the faults continues into the following figure. **Inset:** Topography along A-A' and B-B' transects.

Figure 12. Shaded bathymetry of the offshore part of the Nekor basin. F4 to F17, fault traces; ls, landslides; SB, shelf break; B, bulge; MI, marine incision; black lines, isobaths. Insets: Topography along the A-A', B-B', C-C' and D-D' transects.

Figure 13. Shaded bathymetry of the Trougout Fault zone. SW, sediment waves; F18 to F20, f. : faults.

Figure 14. A. Schematic structural map of the recent tectonic structures of the Nekor basin. PDZ: Principal Displacement Zone; red faults, active faults; thick black arrows, horizontal stress direction; σ_H, maximum horizontal stress; σ_h, minimum horizontal stress. Abbreviations as in figure 1. **Inset:** direction of the Africa-Eurasia convergence from Palano et al. (2013) **B.** Schematic drawing of the offshore part of the Nekor basin and its adjacent shallowest tectonic structures; T.f., Trougout fault; Black Arrow, horizontal stress direction; Grey arrow, lateral play along strike-slip fault zone; σ_H, maximum horizontal stress; σ_h, minimum horizontal stress. The N049° direction of the basement fault is interpreted from the general trend of the *en echelon* R-shear at the surface **Inset:** Simplified scheme of the Nekor basin. R, R-shear above a sinistral basement fault (dashed line). Grey surface, Africa block; white surface, Betico-Rifian block and the Nekor basin; thick white arrow, direction of elongation of the Nekor basin.

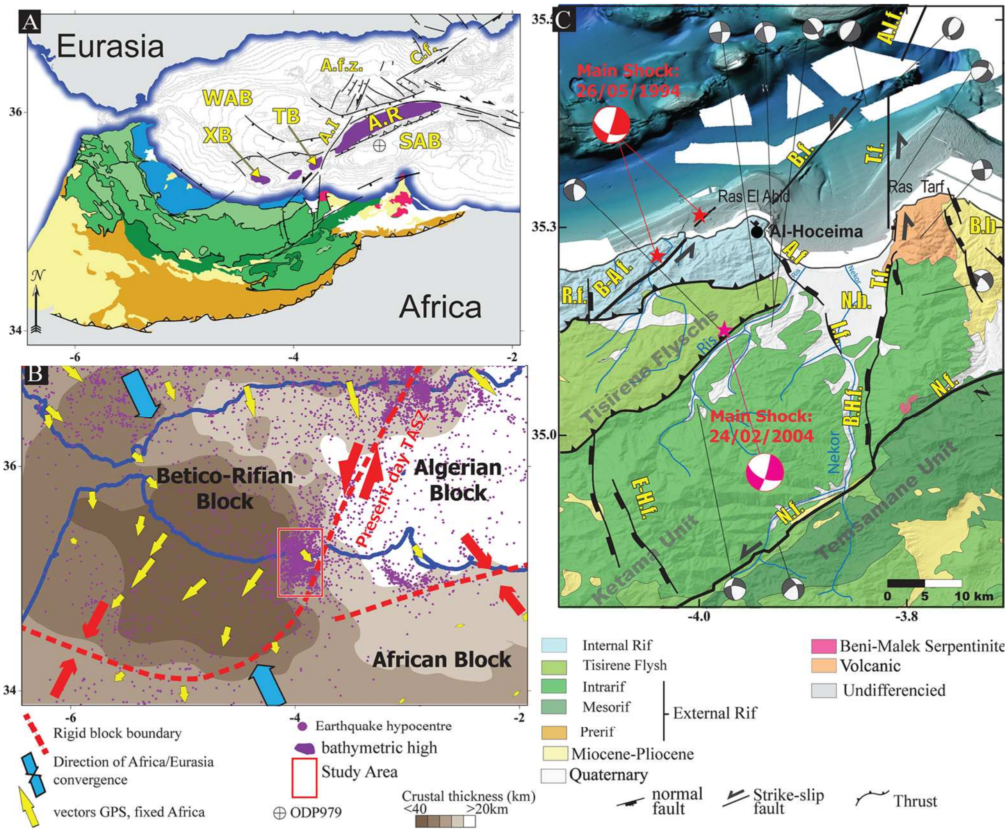

Figure 1. A. Structural map of the Rif onshore and of the Alboran basin offshore modified after Chalouan et al. (2008), Martínez-García et al.(2011), Martínez-García et al. (2013), and Ballesteros et al. (2008). A.f.z., Adra fault zone, A-I.f., Al Idrissi fault; A.R., Alboran Ridge, C., Carboneras fault, SAB, South Alboran Basin; T.B. Tofiño Bank. WAB, western Alboran basin; XB, Xauen bank. B. Kinematics of the Alboran from GPS data (Koulali et al. 2011), associated with the seismicity between 1964 and 2012 (Spanish Instituto Geografico Nacional (IGN) database) and with the thickness of the crust from receiver function redrawn from Mancilla & Diaz 2015; Red arrow, direction of convergence at the rigid block boundaries (Nocquet 2012). C. Regional map of the recent active structures, and shaded relief from the Advanced Spaceborne Thermal Emission and Reflection Radiometer (ASTER) digital elevation model. Swath bathymetry from SARAS and Marlboro-2 cruises (d'Acremont et al. 2014). Focal mechanisms of the 1994 main shock (red star ; El Alami et al. 1998; Biggs et al. 2006) and of the 2004 main shock in violet (van der Woerd et al. 2004). CMT catalog from Bezzeghoud and Buforn (1999). Ras=Cape; A.f., Ajdir fault; B.H.f., Bou Haddad fault; R.f., Rouadi fault, B.f, Bokkoya fault, B.-A.f., Bousekkour-Aghbal fault, I.f., Imzouren fault; T.f., Trougout fault; A.I.f., Al-Idrissi fault; N.f., Nekor fault, E-H.f., El-Hammam fault; N.b., Nekor basin; B.b., Boudinar basin. After Aït Brahim et al. (2004), Medina (1995), Calvert et al. (1997), El Alami et al. (1998), Medina & El Alami (2006), and van der Woerd et al. (2014). The thick crust under the Rifian orogenic arc corresponds approximatively to the area of coupling between the Alboran slab and the Rifian crust (e.g. Perouse et al. 2010; Thurner et al. 2014).

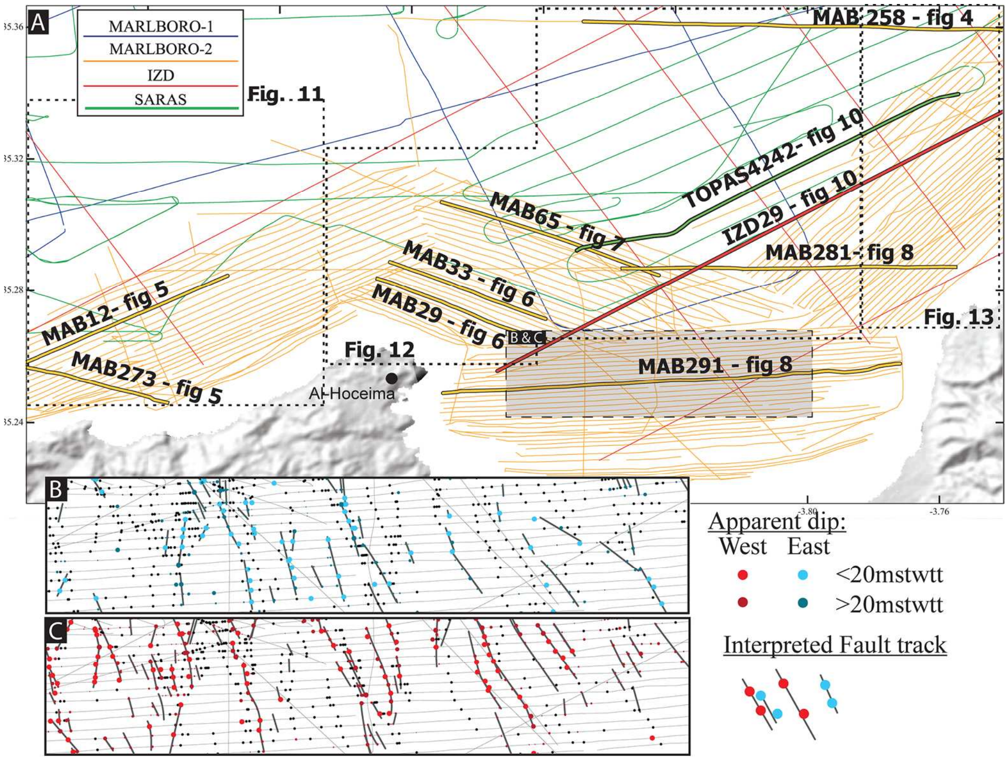

Figure 2. A. Map of the seismic surveys tracklines. Thick line: seismic profiles shown in this studies. Dashed rectangles correspond to focuses on the bathymetry shown in this study. B&C Extract of all of the east (blue dots) and west (red dots) dipping faults spottedon the seismic profiles. Thick lines: interpreted fault traces.¬ The black dots in the insert B show the west dipping faults and conversely the black dots in the insert C show the east dipping faults.

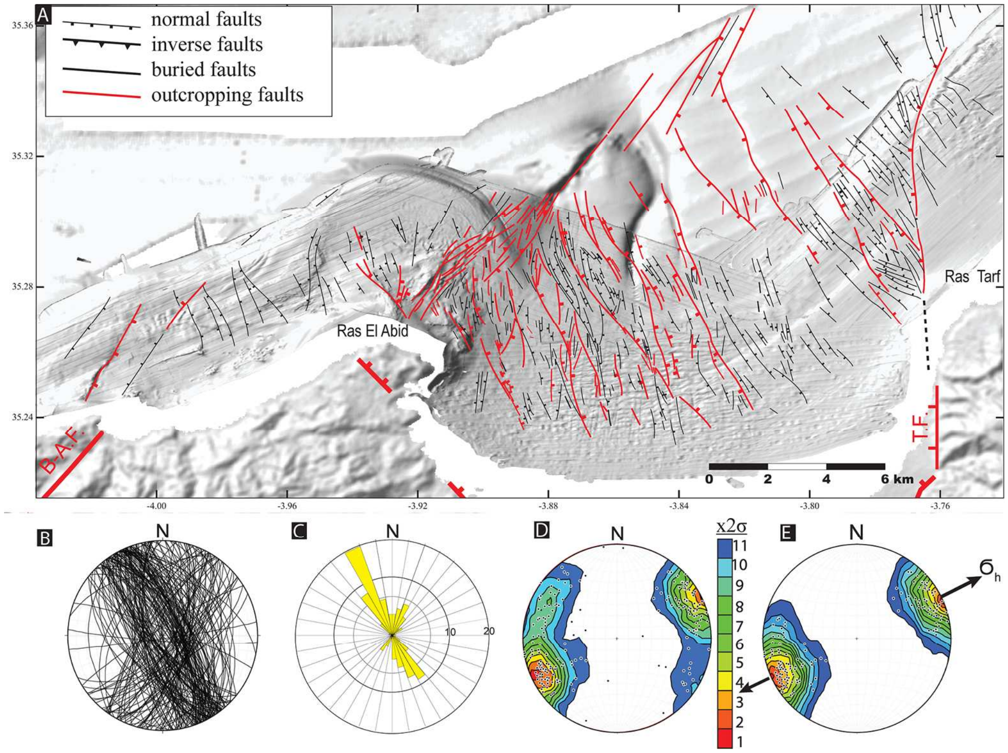

Figure 3. A. Interpreted structural map of the study area overimposed on the shaded bathymetry. B. Lower-sphere stereographic projection of the fault dataset. C. Rose diagram of the fault azimuths. D. Kamb contouring of the complete fault dataset. N = 193; contour interval = x2σ; counting area = 0.17 of the net area; significance level = x3σ; σ is the standard deviation. E. Kamb contouring of the poles of the normal faults. Stereographic projections of equal area. N = 121; contour interval = x2σ; counting area = 0.17 of the net area; significance level = x3σ. Designed with the help of Stereonet 8 (Allmendinger et al., 2012; Cardozo & Allmendinger, 2013). σh: minimum horizontal stress direction. The red area indicates two standard deviations of poles azimuts.

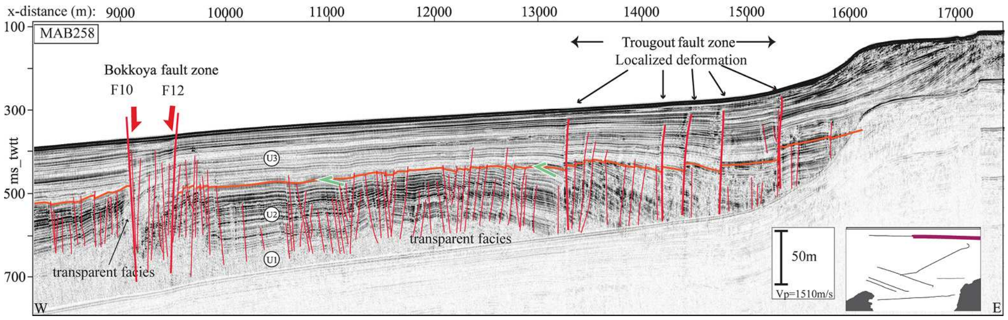

Figure 4. MAB258 seismic reflection profile from the Marlboro-2 survey. Green arrows, toplap; orange reflector, unconformity surface dated around 0.79My. Vertical exaggeration = 10. U1, U2, U3: formations defined from acoustic facies (see main text).

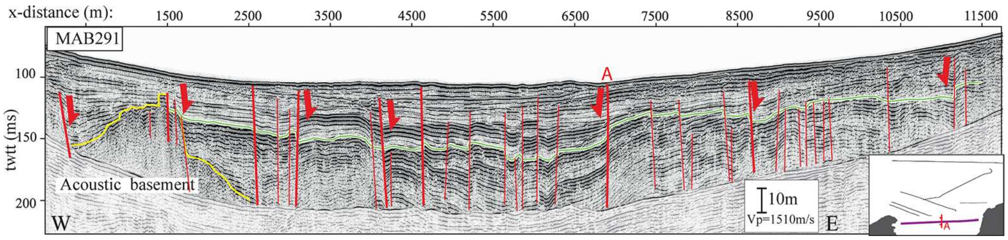

Figure 5. MAB291 seismic reflection profile from the Marlboro-2 survey. Green reflector, erosive surface. Note the truncated faults on the eastern part of the basin. Note the west-dipping fault A which bounds the east of the depocentre above the green surface. Vertical exaggeration: 10. green reflector : top of the pre-extension formation.

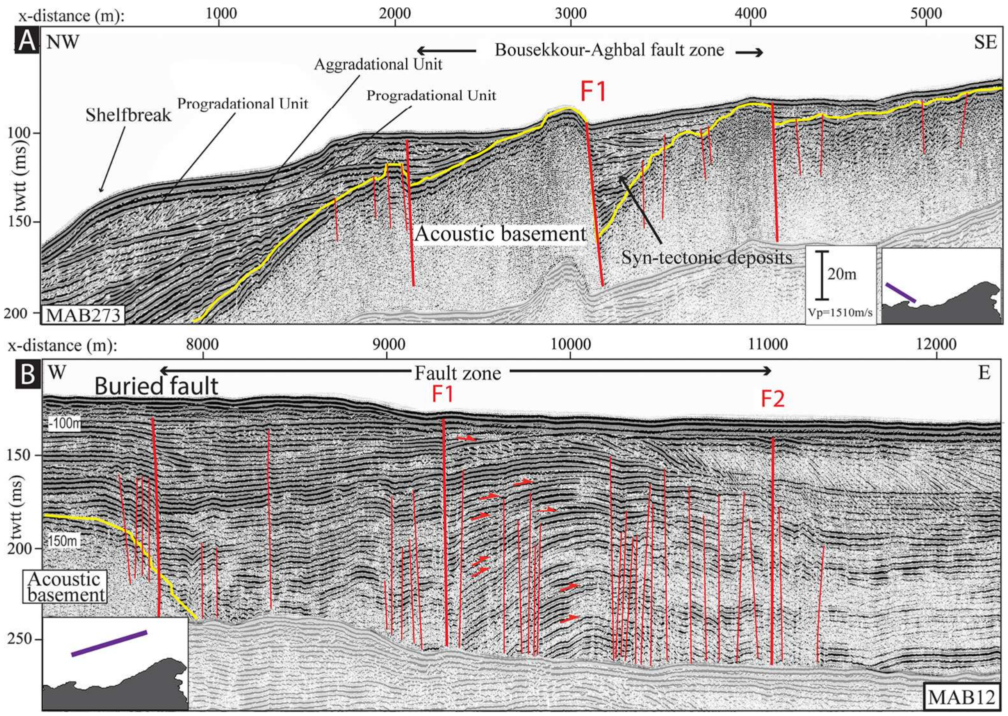

Figure 6: A. MAB273 seismic profile. B. MAB12 seismic profile. Yellow dashed line: top of the acoustic basement; thin red line: non-outcropping faults; thick red line, outcropping fault; red arrows, onlap termination and syn-sedimentary deposits during the growth of the fold; F, fault. The shallow seafloor prevents the imaging of the deeper part of the basin. White transparent mask, multiples; F1 and F2, fault number (see fig. 11). yellow reflector, top of the pre-extension formation; Insets: Position of the seismic profiles on a synthetic map; vertical scale using a velocity of P-waves values equals to 1510m/s. Vertical exaggeration = 10 for the sea-bottom, assuming Vp in water = 1510 m/s.

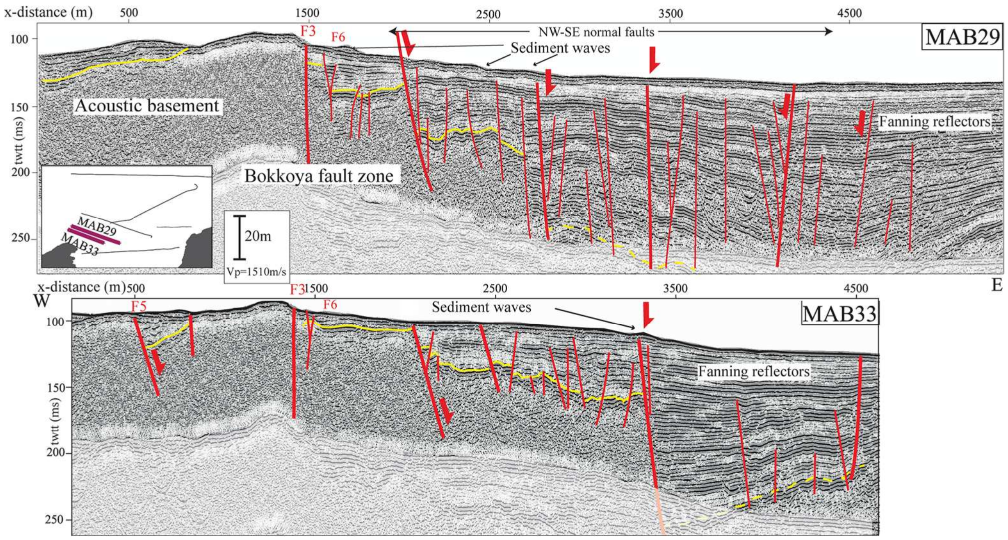

Figure 7. Seismic reflection profiles MAB29 and MAB33 from the Marlboro-2 survey. Thick red lines, major faults at the basin scale; thin red lines, secondary faults; red arrows, apparent vertical motion along fault planes; yellow reflector, top of the pre-extension formation; shaded area, first multiples. F3 to F8, fault number (see fig. 12). Vertical exaggeration = 10

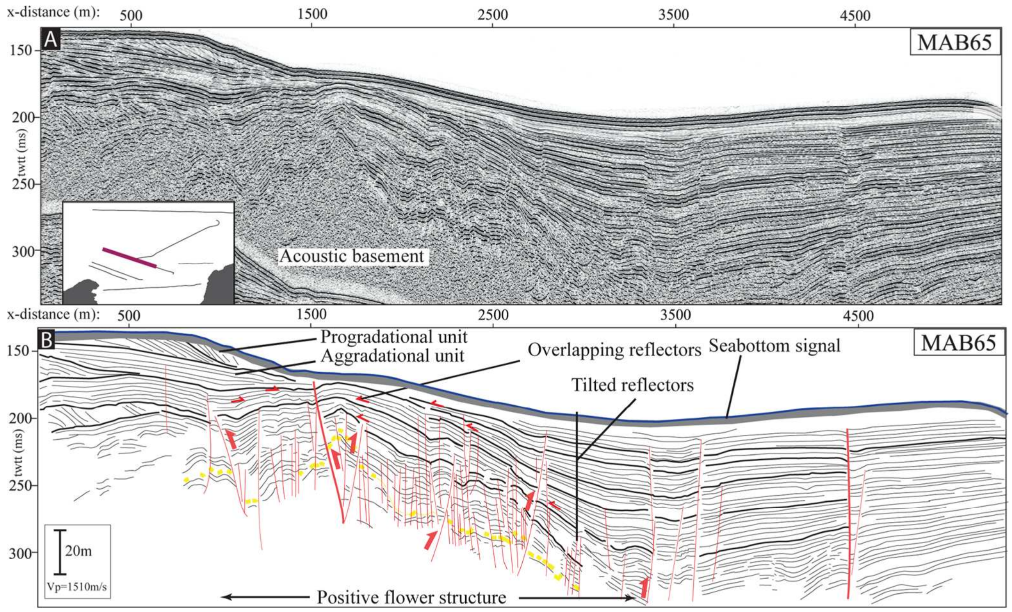

Figure 8. A. MAB65 uninterpreted seismic reflexion profile from the Marlboro-2 survey. Vertical exaggeration: 10. B. Line-drawing of the MAB65 profile. Small arrows, multiple discordances inside the sedimentary record. Faults: same as for Figure 12

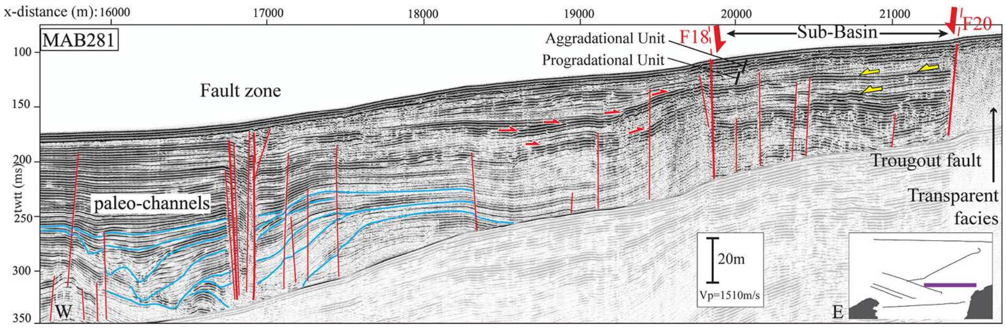

Figure 9. MAB281 seismic reflection profile from the Marlboro-2 survey. Vertical exaggeration = 9.5; blue line, bottom of the incised paleo-channels; red arrows, onlap; yellow arrows, downlap.

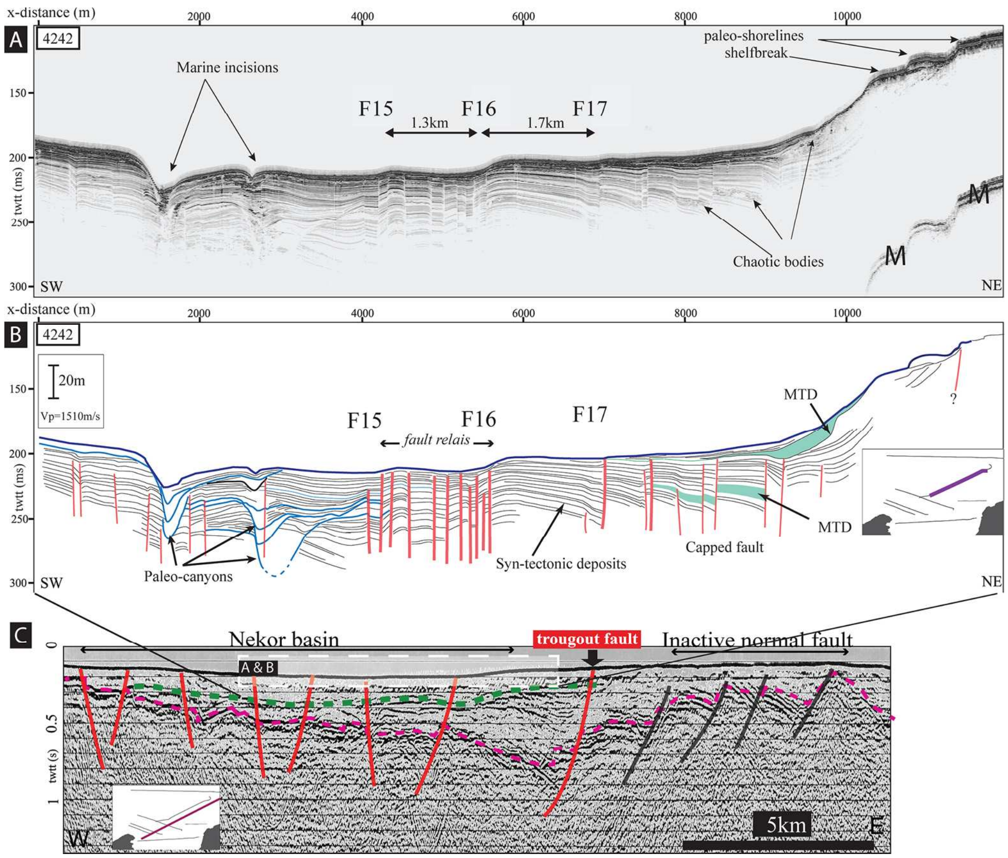

Figure 10. A. TOPAS profile 4242 from the SARAS survey. B. Line drawing of TOPAS profile 4242. Vertical exaggeration = 21; M, Seafloor first multiple. Inset: Topography along the A-A’ transect. See fig. 12 for location of F15 to F17. C. IZD29 profile, modified after Calvert et al. (1997). Dashed purple reflector, bottom reflector of the basin; dashed green reflector, first multiple of the seafloor; red line, faults affecting the bottom reflector of the basin in the Nekor basin; black lines, faults with no imprint on the bathymetry. The position of the TOPAS4242 seismic profile is approximatively projected on the IZD29 seismic profile.

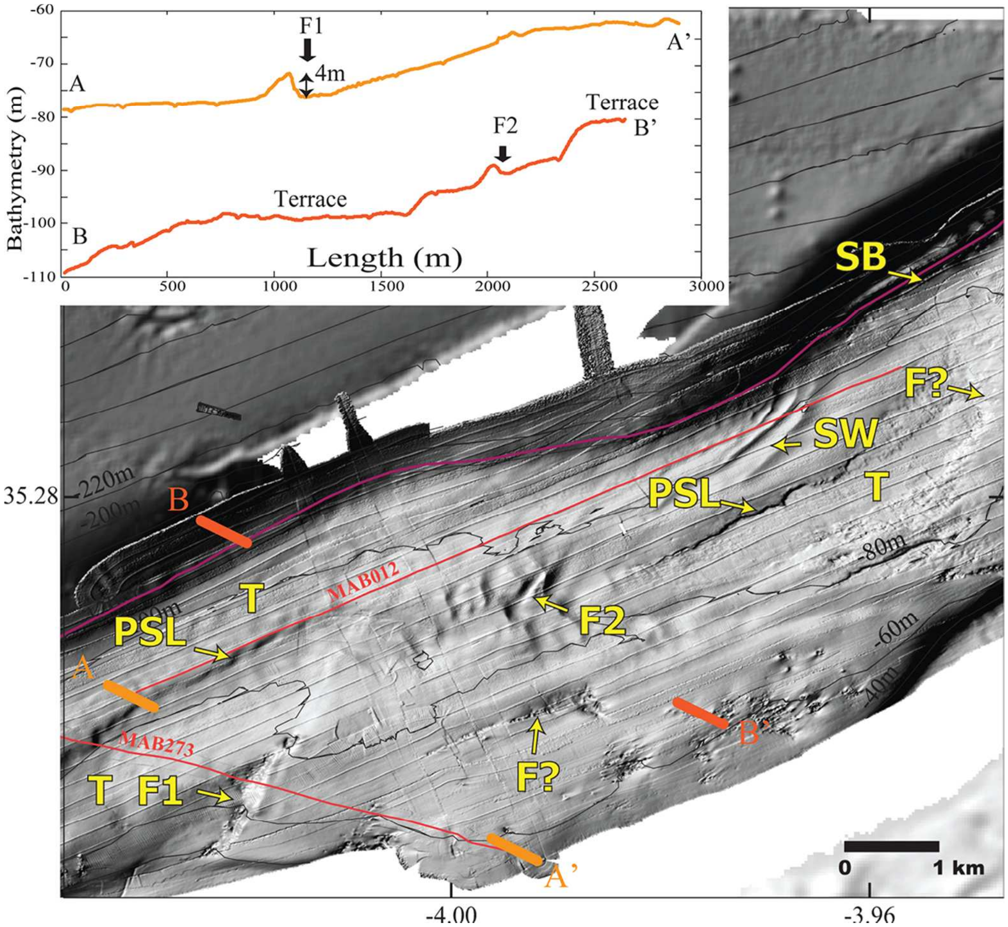

Figure 11: Shaded relief bathymetric map showing the continuity of the Bousekkour-Aghbal fault. F1, F2, faults; PSL, paleo-shoreline; T, terrace; SB, shelf break; dark orange lines, positions of the seismic profiles (see Fig. 2); black lines, isobaths. The purple line indicates the -125m isobath. The numbering of the faults continues into the following figure. Inset: Topography along A-A' and B-B' transects.

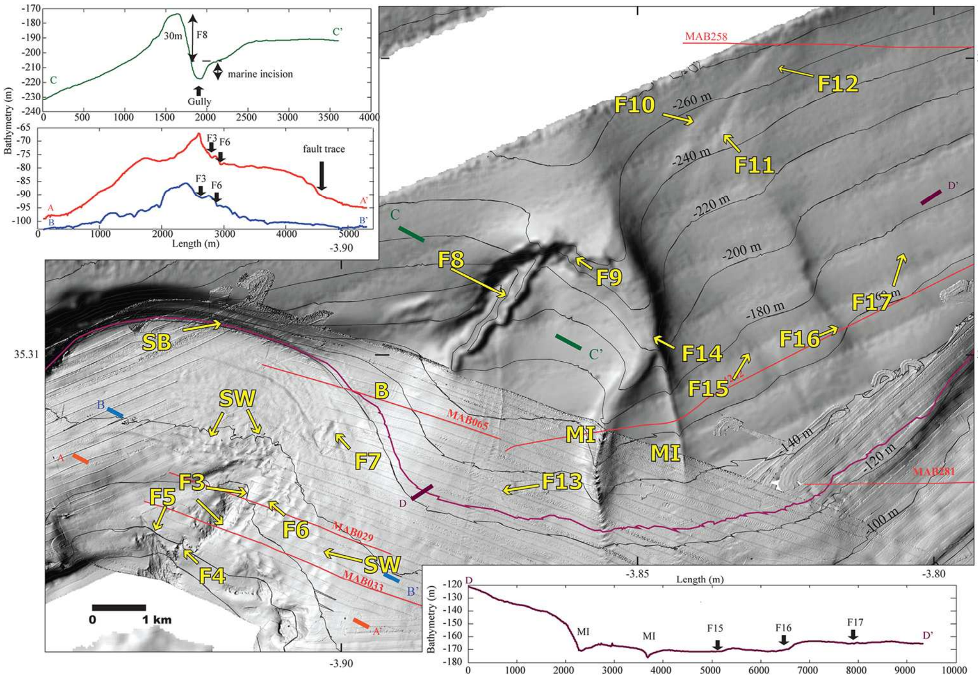

Figure 12. Shaded bathymetry of the offshore part of the Nekor basin. F4 to F17, fault traces; ls, landslides; SB, shelf break; B, bulge; MI, marine incision; black lines, isobaths. Insets: Topography along the A-A', B-B', C-C' and D-D' transects.

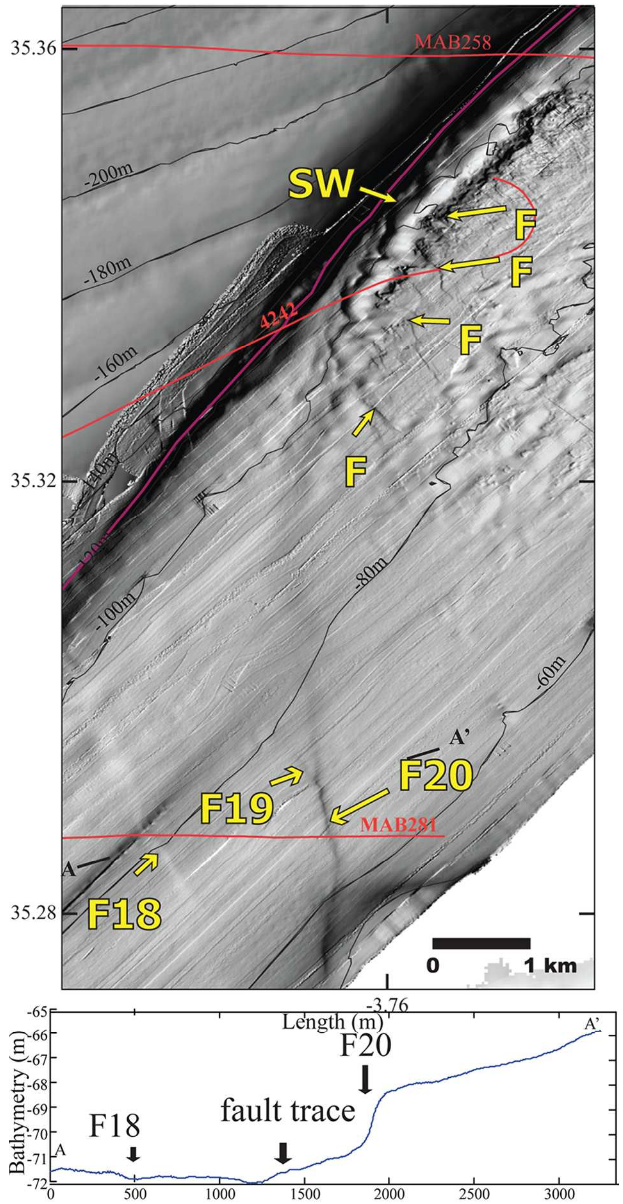

Figure 13. Shaded bathymetry of the Trougout Fault zone. SW, sediment waves; F18 to F20, f. : faults.

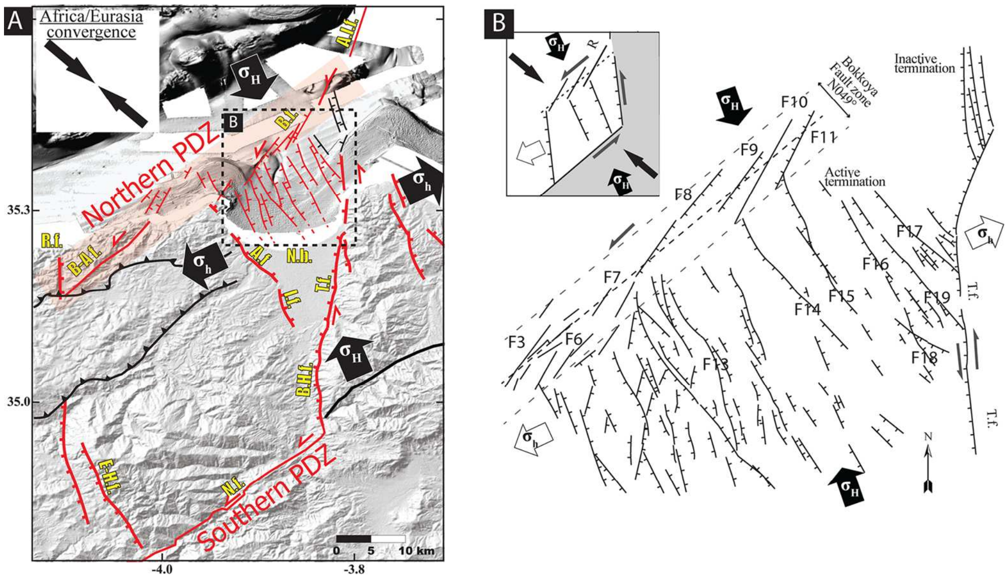

Figure 14. A. Schematic structural map of the recent tectonic structures of the Nekor basin. PDZ: Principal Displacement Zone; red faults, active faults; thick black arrows, horizontal stress direction; σH, maximum horizontal stress; σh, minimum horizontal stress. Abbreviations as in figure 1. Inset: direction of the Africa-Eurasia convergence from Palano et al. (2013) B. Schematic drawing of the offshore part of the Nekor basin and its adjacent shallowest tectonic structures; T.f., Trougout fault; Black Arrow, horizontal stress direction; Grey arrow, lateral play along strike-slip fault zone; σH, maximum horizontal stress; σh, minimum horizontal stress. The N049° direction of the basement fault is interpreted from the general trend of the en echelon R-shear at the surface Inset: Simplified scheme of the Nekor basin. R, R-shear above a sinistral basement fault (dashed line). Grey surface, Africa block; white surface, Betico-Rifian block and the Nekor basin; thick white arrow, direction of elongation of the Nekor basin.